Final Technical Report

Development of Surface Engineered Coating Systems for Aluminum Pressure Die Casting Dies: Towards a 'Smart' Die Coating

DOE Award Number: DE-FC36-04GO14230

Project Period: January 1, 2004 – June 30, 2012

Principal Investigators:

PI: John J. Moore, 303-273-3771, jjmoore@mines.edu

Co-PI: Jianliang Lin, 303-273-3178, jlin@mines.edu

Recipient organization:

Colorado School of Mines, Golden, CO 80401 USA

July 2012

Proprietary Data Notice: None in this report.

The development of surface engineered coating systems for aluminum pressure die casting dies: towards a 'smart' die coating

DOE # DE-FC36-04GO14230

Final Report

Table of Contents

List of Acronyms

ACSEL (Advanced Coatings and Surface Engineering Laboratory)

ATI (Advanced Technology Institute)

CFUBMS (Closed field unbalanced magnetron sputtering)

COF (Coefficient of friction)

CSM (Colorado School of Mines)

CTE (Coefficient of thermal expansion)

FESEM (Field-emission scanning electron microscope)

GDOES (Glow discharge optical emission spectrometry)

GIXRD (Grazing incident X-ray diffraction)

NADCA (North American Die Casting Association)

SAED (Selected area electron diffraction)

TEM (Transmission electron microscope)

XPS (X-ray photoelectron spectroscopy)

XRD (X-ray diffraction)

Lists of Figures

List of Tables

Executive Summary

The main objective of this research program was to design and develop an optimal coating system that extends die life by minimizing premature die failure. In high-pressure aluminum die-casting, the die, core pins and inserts must withstand severe processing conditions. Many of the dies and tools in the industry are being coated to improve wear-resistance and decrease down-time for maintenance. However, thermal fatigue in metal itself can still be a major problem, especially since it often leads to catastrophic failure (i.e. die breakage) as opposed to a wear-based failure (parts begin to go out of tolerance). Tooling costs remain the largest portion of production costs for many of these parts, so the ability prevent catastrophic failures would be transformative for the manufacturing industry.

A smart coating design based on thin film piezoelectric sensor embedded within a tribological coating system has been introduced. By comparing with the homogeneous and graded coating architecture, CrN/AlN superlattice film has been identified as the optimized tribological layer. CrN/AlN superlattice films deposited using pulsed closed field unbalanced magnetron sputtering have demonstrated superhardness (>40 GPa), excellent hardness/elastic modulus (H/E) ratios (an indirect measure of toughness of the coating), good adhesion and oxidation resistance. AlN has been identified as the smart thin film because of its high Curie temperature, high electrical resistivity, and high thermal conductivity making it ideal for high temperature applications. It was found that in order to achieve the best piezoelectric performance from an AlN layer, it is important that the c-axis of the hexagonal crystal structure be oriented perpendicular to the substrate. AlN thin films deposited using pulsed closed field unbalanced magnetron sputtering have demonstrated good piezoelectric response and excellent thermal stability.

The technology offers energy savings through reduced energy use in the die casting process from several factors, including increased life of the tools and dies, reuse of the dies and die components, reduction/elimination of lubricants, and reduced machine down time, and reduction of Al solder sticking on the die. The use of the optimized die coating system will also reduce environmental wastes and scrap parts. Current (2012) annual energy saving estimates, based on initial dissemination to the casting industry in 2010 and market penetration of 80% by 2020, is 3.1 trillion BTU's/year. The average annual estimate of CO_2 reduction per year through 2020 is 0.63 Million Metric Tons of Carbon Equivalent (MM TCE).

In an effort to commercialize the developed coatings, the optimized coatings have been reproduced by industry partners using industrial sized equipment. The coated die core pins have been tested in Al die casting in-plant trials. Significant enhancement in the die life and die casting performance were demonstrated with the optimized coating system. However there remain two major commercialization challenges: 1) Significantly reduce the production cost of the 'smart' coating system; and 2) obtain in-situ piezoelectric signal using remote control during the real die casting process.

1. Introduction

The research philosophy adopted in this research program is the design and development of an optimal "coating system" that ultimately extends die life by minimizing premature die failure. There is a great need to develop advanced surface engineering coating systems that provide superior protection for die and die components from harsh operating environments (oxidation and corrosion resistance), coupled with high hardness, good wear resistance, and increased toughness. It is also essential that catastrophic failure of the coating be prevented by monitoring the stresses and micro-cracks generated in the coating during its service life. It is postulated here that these two functions can be achieved by depositing films that use an engineered 'smart' AlN thin film sensor incorporated into a superhard and tough CrN/AlN based nanolaminate coating system. The smart layer is a piezoelectric AlN thin film that has been selected for its high thermal stability in addition to good electrical properties such as high band gap, high resistivity, and excellent piezoelectric voltage response. Protecting the smart-layer and the customer's tool, die, or component beneath, would be a nano-multilayer, or 'superlattice' coating that is harder and tougher than almost any PVD/CVD coating available today.

There are three main objectives of the proposed work. The first is to optimize the superhard and tough CrN/AlN nanolaminate coating system through the fundamental experiments and in plant trials. The second objective is to design and optimize an AlN thin film sensor. The third is to work closely with industry partners, e.g. North American Die Casting Association (NADCA), Advanced Technology Institute (ATI), Phygen Coating, Inc., etc., to stimulate the transfer of knowledge from academia to industry.

The proposed research has the potential to improve significantly the life and performance of die and die components in high pressure die casting. Meanwhile, the research project provides a more fundamental understanding and knowledge base as to the 'smart' piezoelectric thin film sensor, which has great potential to be used for many applications, e.g. stress sensor for cutting tools, aircraft, automotive, etc. The energy and cost saving impact is of great profit, e.g. high efficiency die casting process; improved lifetime and durability for the dies, reduced machine downtime and cycle time, etc,. Training skilled and qualified surface engineers in this new technology will speed up its adoption and advancement into the US manufacturing industry.

2. Background

2.1 Die Casting and Die Coating Failure

Die casting is an important metallurgical process, which produces geometrically complex metallic parts with excellent surface finish at a low scrap rate. Four principal alloy families are commonly die cast: Al, Zn, Mg, and Cu-base alloys. The interaction of the die and the surrounding environment (liquid metal, oxidation, and wear at elevated temperature) plays an important role in initiating soldering, micro-cracking, crack propagation and finally catastrophic failure. Die failure is a significant issue in die casting which results in considerable energy consumption and wastage. The greatest cost to the die caster is the replacement of the dies, e.g. $20,000-$200,000 for each new die. Another consideration is environmental and energy waste incurred every time the die material prematurely fails, and the consequent cost of down time in production. The major mechanisms leading to premature die failure include (not limited to) thermal cracking (heat checking), erosive wear, soldering, and corrosion/oxidation [1].

Hard coatings have been used for die protection for several years. Most of these coatings are based on various nitride, boride, oxide or carbide compounds, e.g. TiN, TiAlN, SiC, BN, TiC, Al_2O_3, etc [2, 3]. The existing surface treatment and coating technologies to protect the die surface do extend the lifetime of a die, but the die often fails catastrophically with little warning to the operator and has to be replaced with major cost and machine shut down disadvantages. It was found that the most catastrophic failure of die coatings is the thermal fatigue attack from the large thermal and mechanical stresses generated during the die casting process [4]. Thermal stresses arise from differences of coefficient of thermal expansions (CTE mismatch) creating intrinsic stress within the die material. Mechanical stresses come from pressure within the casting material being pressed against the die. Thermal fatigue cracking (heat checking) is generated by the release of the accumulated thermal residual stress within the brittle ceramic-based coatings, which is formed by the mismatch of the coefficient of thermal expansion (CTE) between the surface coating and the die substrate during alternating heating and cooling cycles. As soon as cracks appear in the coating, the aluminum melt penetrates the cracks and directly contacts the die substrate forming brittle Fe-Al-Si ternary intermetallics that fracture leaving a defect in the die surface. There is mismatch in thermal expansion even when zinc and magnesium are cast, however this work focused on aluminum since aluminum makes up the bulk of the die casting shipments. The conjoint action between the thermal fatigue cracking and

chemical attack intensifies the degradation of the coating and H13 substrate [1,5].

It is postulated that both types of stress can be avoided by creating an optimized surface engineered hard coating to extend the life of the die. In addition to this protective layer, a piezoelectric layer is desired to see where the stresses arise as well offer a direct measurement of the working temperature at the die level.

The thermal fatigue resistance of hard coatings is related to the ability to accommodate the thermal stress within the coatings, which is directly determined by the toughness and the architecture of the coatings [6]. Using multilayered and graded design architecture of the coatings is a promising approach to minimize the thermal fatigue failure and significantly increase the toughness and lifetime of the coating and decrease deterioration of the die substrate. As shown in **Figure 1**, for monolithic coatings, thermal fatigue cracking is initiated at the coating surface, and the cracks can easily propagate perpendicular to the substrate. However, these cracks can change their propagation directions at layer interfaces if the coating is designed with a graded or multilayer system. Another important benefit of multilayer coating systems is that it can provide a consistent 'accommodation' of the thermal stresses that developed from thermal cycling, and can minimize the mismatch of CTE and stresses inherent in the coating system.
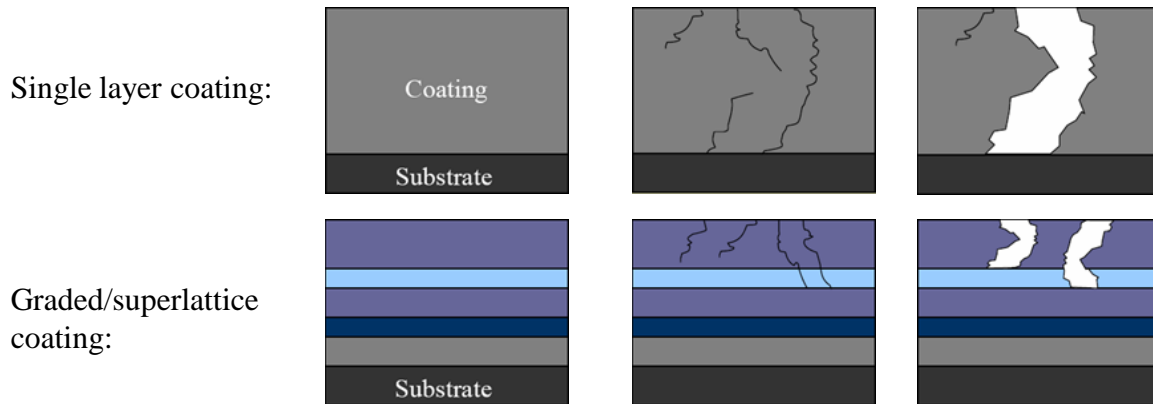
Figure 1 Schematically Drawing shows the Thermal Cracks Propagation within Single Layer and Grade/multilayer Coatings

2.2 Nanoscale Multilayer Coatings

Recent advances in the coating design made it possible to obtain nanostructured composite thin films and coatings that exhibit outstanding multifunctional properties to meet a wide range of demands including high hardness, good toughness, better adhesion, chemical inertness, and good thermal stability, in comparison to traditional monolithic/single-phase

coatings. Nanoscale multilayer coating is a typical example.

The nanoscale multilayer composite coatings comprise alternating layers of two or more different materials with controlled modulation period (Λ) in the nanometer scale. The layers can be constructed by metal/metal layers (e.g. Al/Cu [7]), metal/ceramic layers (e.g. Ti/TiN, W/WN [8]) and more often the ceramic/ceramic layers (e.g. TiN/NbN [9],TiN/VN[10], CrN/NbN [11], CrN/AlN [12,13], CrN/TiN [14]). Early research by Palatnik with multilayer of metals showed that significant improvements in strength were achieved when layer thickness was decreased below 500 nm [15]. In early modeling, Koehler [16] predicted that high shear strength coatings could be produced by alternating layers of high and low elastic modulus. Key elements of the concept are that very thin layers ($\leq$ 10 nm) inhibit dislocation formation, while differences in elastic modulus between layers inhibit dislocation mobility. To achieve increased strength, the layers must have sharp interfaces and periodicity in the 5-10 nm range. If the layers are not of the correct periodicity, the benefits will be lost. The Advanced Coatings and Surface Engineering Laboratory (ACSEL) at the Colorado School of Mines (CSM) has developed a wide range of nanoscale multilayer coating systems, e.g. CrN/AlN, TiBCN/CNx, TiN/CrN, MCrAl/Al, as shown in **Figure 2**, which exhibited super hardness (>40 GPa), high toughness, superior wear, corrosion, and oxidation resistance under harsh working conditions [17, 18, 19, 20]. These multilayer coating systems have been successfully used for cutting tool and die casting applications, to meet multiple functions as required by the harsh working conditions. Preliminary research at the ACSEL have identified that the nanoscale multilayered CrN/AlN coatings has shown improved hardness, wear resistance, thermal resistance and toughness as compared to traditional die coatings and surface treatments. The structure and properties of the nanoscale multilayer coatings strongly depend on the coating architecture design in terms of the composition, layer thickness, multiphase selection, and grain size.
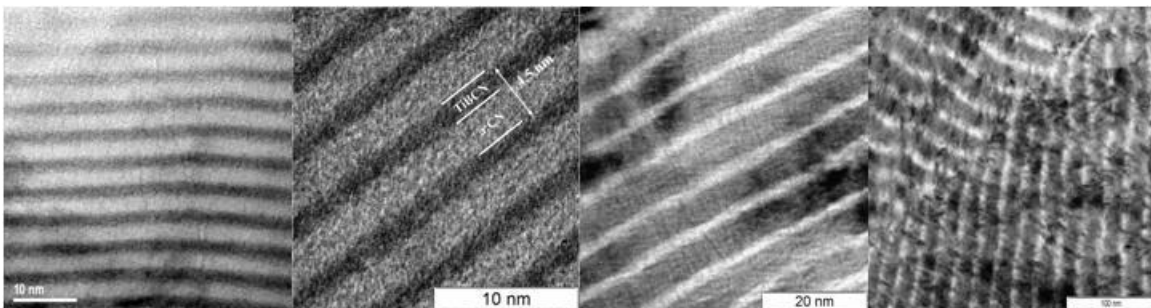
Figure 2 Cross-sectional TEM images of nano-scale multilayer coatings synthesized in ACSEL labs: (a) CrN/AlN, (b) TiBCN/CNx, and (c) TiN/CrN, and (d) MCrAl/Al

2.3 Design Concept of the Surface Engineered 'Smart' Coating System

As mentioned before, the catastrophic failure of the die coating and dies is mainly due to the thermal fatigue attack from the large thermal and mechanical stresses generated during the die casting process. To further improve the performance and multifunctionality of the coating system to meet current aggressive environments for metal forming applications, there is an emerging need in the design and use of an engineered 'smart' thin film sensor incorporated within the overall die coating system.

The primary functions of this 'smart' die coating system contain two aspects:

i) Improved new performance: The coating system will be optimized with respect to achieving non-wetting with the liquid casting metal, wear and oxidation resistance, and coupled with delay of onset of thermal fatigue cracking (heat checking).

ii) 'Smart' capabilities: The coating system is capable of indicating the initiation of micro cracks and crack propagation in die coatings and die components by monitoring the stresses generated in the die coating, so that the operator can use this system efficiently and effectively.

To achieve the above goals, a thin film piezoelectric sensor will be embedded into an optimized nanoscale multilayer tribological die coating to form an overall 'smart' die coating system. A schematic diagram of the 'smart' die coating architecture specifically designed for use in aluminum pressure die casting is presented in **Figure 3**. The tribological coating system containing a working layer and a nanoscale multilayered or compositionally graded intermediate layer, will provide the overall coating system a suitable combination of properties of non-wetting with the liquid aluminum, wear and oxidation resistance, and preferably will delay the onset of thermal fatigue cracking. Two typical technical examples of the nanoscale multilayered or compositionally graded intermediate layer based on a Cr-Al-N coating system are also presented in **Figure 3** [21,22]. For early research projects, a "superlattice" of CrN/AlN tribological coatings shows optimum properties layer which has been selected as the tribological working layer.

The piezoelectric thin film sensor (including the piezoelectric film and the electrodes) will be placed between the top tribological coating system and the bottom ferrtic nitrocarburized H13 die substrate to provide the capability of sensing the initiation of microcracking and crack propagation in the die/die coating by monitoring the internal stresses generated in the die and die coating. In general, strain in the material is increased prior to the initiation of a crack. Once

cracks have been generated there is a decrease in the strain. Therefore by continuous monitoring the strain level in the die coating, this 'smart' coating system can continuously inform the operator and management as to the state of the stress level in the die surface. This knowledge allows the operator to strategically remove the die from production before catastrophic die failure occurs. This offers the potential for considerable savings in terms of die replacement and repair.
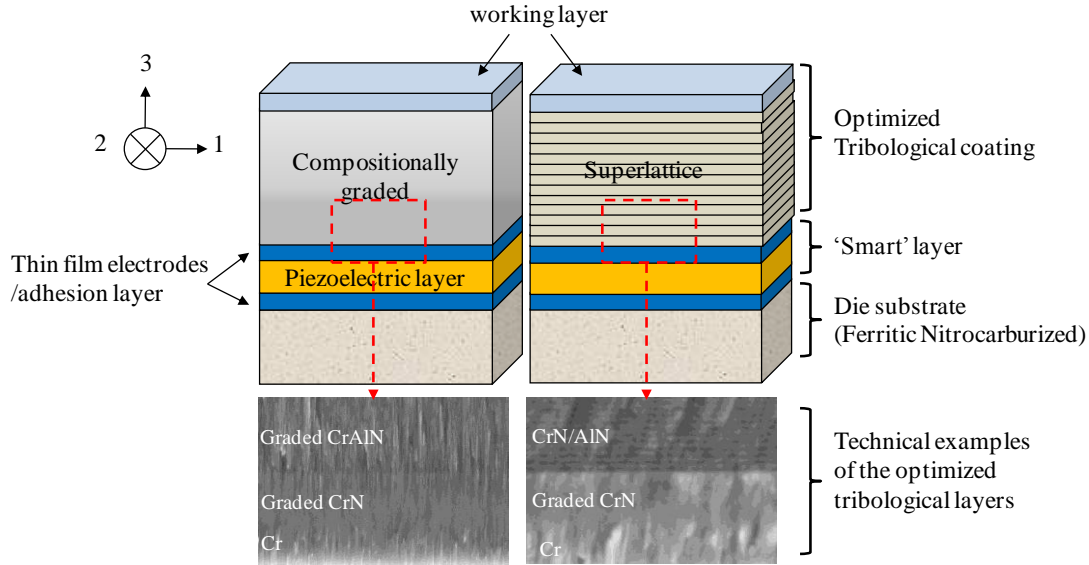
Figure 3 A schematic diagram of the optimized 'smart' coating architecture for die coatings used in aluminum pressure die casting

2.4 Piezoelectricity of the Materials

Piezoelectricity was first demonstrated by the Curie Brothers, Jacques and Pierre, in 1880 [23]. Piezoelectricity is the ability of materials to produce an electric charge in response to applied mechanical stress (the material is squeezed or stretched) [24]. In the current 'smart' coating design, the sensor element is a small piezoelectric thin film. The deformation of the unit crystal under mechanical stress parallel to its sides changes the charge distribution inside the unit cell thus producing a dipole moment throughout the entire sample, as illustrated in **Figure 4**. These dipoles have a polarization, one end is more negatively charged and the other end is positively charged, therefore leading to the formation of an electrical polarization across the crystal lattice. If the material is not short-circuited, the applied charge induces a voltage across the material. If the sensor element is sandwiched between two electrodes, there will be charges developed on the electrode surface, which can be collected as an output signal by the electronic system.

The associated voltage in piezoelectric materials has been found to be proportional to the magnitude of mechanical stress. The proportionality constant is given by the piezoelectric constant, ε_{31}, as described in this simple relation:

$$V = E.d = \varepsilon_{31}.\sigma_{12}$$

where, E is the electric field, d is the thickness of the film, σ_{12} is the stress, the indices 1, 2 ,3 stand for the X,Y and Z axes, the X-Y plane being parallel to the die/die coating interface at a particular point, as indicated in Figure 1.
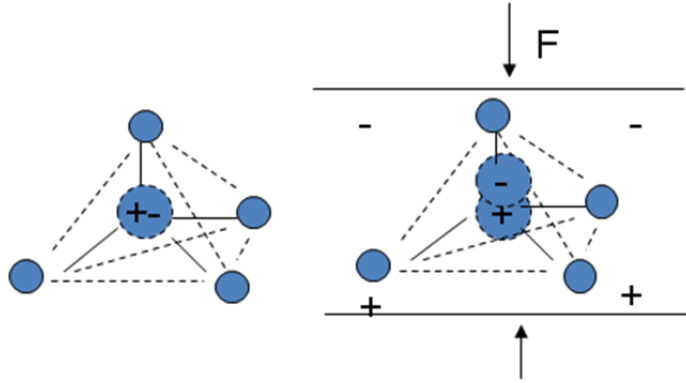
Figure 4 Polarization of dipoles in crystals under mechanical stress to generate piezoelectric effect.
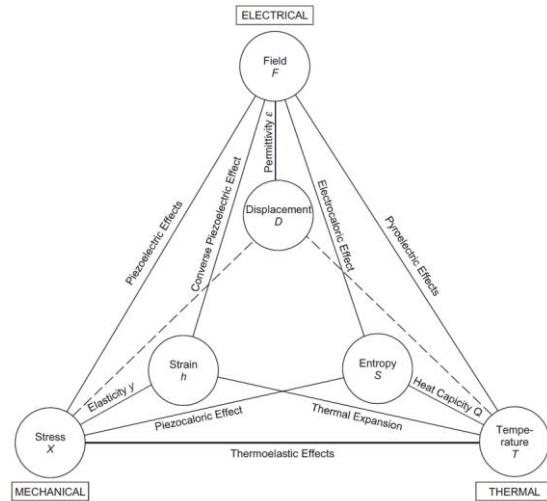
Figure 5 The relations between physical domains [25]

To understand what the piezoelectric effect really is, one needs to understand the fundamental relationship between physical domains. **Figure 5** shows how each physical domain is linked to the others by the physical response associated with transition [25]. For example, a thermal stress translates to mechanical strain via the coefficient of thermal expansion.

As noted before, the piezoelectric effect can be defined as the link between mechanical stress and electric response. Yet it is important to note that the piezoelectric effect can further be divided to the direct and converse effects. As seen above, the direct effect is described as a mechanical stress causing an electric response, whereas the converse comes from applying an electric potential and achieving a mechanical response. It is quite important to note that these relationships and effects do not occur in all materials, in fact very few. The most relevant property of this type of material includes storing a permanent charge or field due to a permanent dipole moment. This dipole comes from a crystal structure that does not have a center of symmetry, i.e. a non-centrosymmetric crystal structure. Having this non-symmetric lattice creates an imbalance of charge within the unit cell causing the dipole necessary to store the charge. The main problem with these materials is that they require a specific phase to accomplish this non-centrosymmetric structure and thus their piezoelectric properties. This is discussed in the next section. The most common crystal structures for piezoelectric materials are in the form of Perovskite and Wurtzite. Perovskite is the generic name for structures having two metal cations and oxygen as the anion. At room temperature, the negatively charged oxygen creates a polarization by the metal cation shifting. The Wurtzite structure is not cubic but hexagonal close packed. Materials in the Wurtzite structure are generally binary compounds where each of the atom types bond and make the hexagonal sub-lattice.

Beyond crystal structure, some key differences between the Perovskite and Wurtzite structures exist. Wurtzite materials tend to have one to two orders of magnitude lower piezoelectric constant, yet remain viable materials due to their hysteresis free response [26], high temperature range, and easier fabrication. They also tend to have higher Young's moduli, providing more rigid and structurally sound films. Wurtzite films can be deposited via CVD or PVD (sputtering or PLD), whereas Perovskites can be made via, CVD, PVD, sol-gel, and traditional sintering. To compensate for the lower piezoelectric constant, highly textured films are necessary, and are done so through deposition techniques discussed shortly.

iezoelectric materials are highly temperature sensitive. For Perovskite structures, at room temperature they exhibit a tetragonal structure, which is ferroelectric, whereas above their Curie temperature they exhibit a cubic or orthorhombic paraelectric phase. Paraelectric materials do not keep their polarization after the field is removed, whereas ferroelectric materials do. Wurtzite structures are also affected in this same manner, losing their polarization

and thus piezoelectric properties at temperatures above the Curie point. So when designing the 'smart' layer, a material must be chosen that will function under the operating conditions without failure.

It is possible to detect the instantaneous stress by embedding a piezoelectric sensor within the structure. The embedded piezoelectric thin film sensor has the capability of sensing the initiation of micro- cracking and crack propagation by monitoring the internal stresses generated within the materials. Usually, strain in the material is increased prior to initiation of a crack and once the cracks have been generated, there is a drop in the strain level due to strain/stress relief accompanying the generation of the crack, which could be controlled continuously by the incorporation of a smart structure in the system. The signal carrying wires, however, have to be insulated from the body as well as from each other, and that is why a high temperature non-piezoelectric insulator should coat the sensor element with the top and bottom electrodes. The reason for this requirement is to avoid charge leakage through electrical conduction, and that is why it is extremely important that the active sensor element also should have as little electrical conduction as possible. The resulting irregularity of the surface could result in strong electric field inhomogeneity, the electric field exceeding the breakdown field in some places. These places could initiate an avalanche breakdown throughout the sample. In addition, the scattering between the sputtered atoms/ions could change the incidence angle of the incoming particles to the substrate, and the normal statistical fluctuation in surface height can cause significant shadowing of the non-normal beam and eventually block some places of the substrates from any deposition, which finally leads to a porous film. A porous film can be a potential source for strong electric field concentration in certain places leading to an early breakdown of the sample. Any cavities inside the film would generate high field regions between the voids and at high concentration of the cavity sites, these high field regions could result in total breakdown of the sensor. A schematic representation of these potential electrical failure mechanisms is depicted in **Figure 6a-c**.
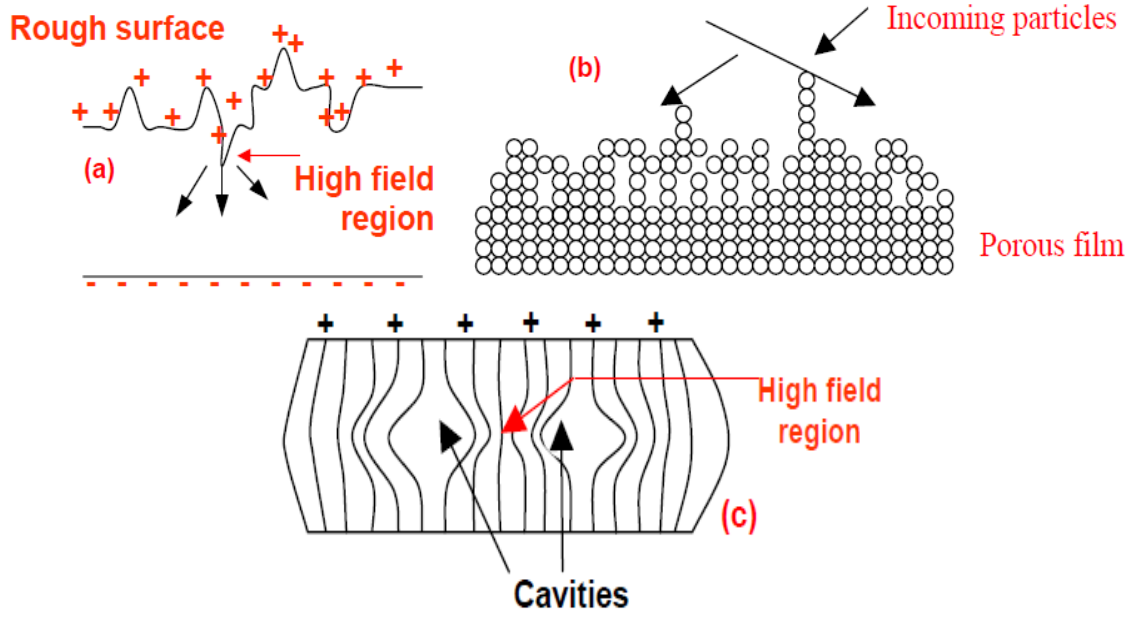
Figure 6 Schematic of the inhomogeneous field distribution within a film containing process induced imperfections

2.5 Sensor Thin Film Materials Selection Criteria

To select the proper piezoelectric candidate for the 'smart' coating sensor, one has to consider the following factors.

i) First of all, the piezoelectric material used in the 'smart' coating sensor must exhibit high piezoelectric constant (ε_{31}) to obtain sufficient piezoelectricity sensitivity in response to the small mechanical stress generated from the internal stress variation within the die coatings. Theoretically, the orientation of the polar axes of the crystal with respect to the acting force determines the magnitude of the charge. Therefore, to obtain the maximum piezoelectric effect in the piezoelectric coating sensor, the orientation/texture of the thin film must be carefully controlled.

i) Electrical conduction through the sensor layer can act as a source of leaking the stress-induced electrical charges through itself, therefore losing the piezoelectric effect. The conduction properties in a thin film structure can be significantly different from that in the bulk form, due to various reasons [27]. The most important factor responsible for this difference is the electric field, which in a thin film is at least 10^3 times larger than the bulk at normal operating voltages. The high electric field induced phenomena can include field-assisted thermionic electron emission from electrodes, and also the space charge controlled current conduction. Consequently, high electrical resistivity of the piezoelectric coating sensor is necessary so that a large electric

12

field can be applied during poling without breakdown or excessive charge leakage at both room and high temperatures. High insulation resistance 'R' is also required during operation of the device. The transducer must not only develop a charge for an applied stress or strain, but must also maintain the charge for a time long enough to be detected by the electronic system.

The microstructure, surface morphology and impurity level in the film together with the operation temperature will strongly affect the resistivity and insulation resistance of the piezoelectric films:

(a) The chemical impurities within the films will result in dangling bonds and hence acting as electron traps that can strongly modify the charge conduction, in general in a positive way.

(b)The presence of cavities would confine the electric field lines inside the high dielectric constant solid regions separating the cavities, and hence increasing the density of field lines in those regions. If the cavities are high in number and if the material has a high dielectric constant, this case can lead to a permanent electrical breakdown of the sample.

(c) The surface also has an important role in determining the homogeneity of the electric field. A small conducting sphere, whose local capacitance would be proportional to its radius, can approximate a protrusion on the electrode surface inside the sample. The local charge density on the protruded region is inversely proportional to the radius of that region. This would imply a high field in the vicinity of a protrusion, and low field near a smooth region. This high local field can very well initiate an electric breakdown, which can propagate through the whole sample. To avoid this type of surface induced breakdown, it is therefore, desirable to have a smooth surface of the sample. Large spherical grains (which often form in a material with isotropic surface energies) are often undesirable due to the formation of deeper grain boundaries. These deep grain boundaries would behave as conducting needles when the sample is coated with an electrode layer.

(d) The high temperature may, however, activate the detrapping process of electrons and aid the charge conduction and a drastic reduction of sample insulation [28].

(iii) Since the whole coating architecture will be used at elevated temperatures (e.g. up to 700°C in Al pressure die casting), the piezoelectric thin film sensor needs to have a suitable electrically stable temperature range, which can be evaluated by the Curie temperature. The Curie temperature is defined as the critical temperature at which the crystal structure changes

from a non-symmetrical (piezoelectric) to a symmetrical (non-piezoelectric) form when the piezoelectric thin film is expressed in evaluated temperatures. It should be noted that the transition from a piezoelectric to a non piezoelectric stage is not necessarily an abrupt transition for many materials, but can begin from well below the Curie temperature as manifested by a temperature dependent change in polarization, also known as pyroelectricity. This polarization change may interfere with the stress induced polarization change, and complicate the signal recovery.

(iv) From a practical point of view, the piezoelectric thin film layer must exhibit good compatibility with the die substrate and the top tribological coating to ensure good adhesion of the overall coating system and avoid creating artificial defects and stresses at the interfaces. For example, the coefficient of thermal expansion (CTE) of the piezoelectric material needs to be considered for calculating the intrinsic thermal stress built into the 'smart' die coating system because of possible CTE mismatch between adjacent materials. Other requirements for the piezoelectric thin film sensor include stable mechanical and electrical properties over a wide temperature range and a long service life, which is also significantly determined by the proper selection of the material and for structure and property control.

Oxide-based pyroelectric and ferroelectric materials have the general formula ABO_3 and are employed for their dielectric, piezoelectric, pyroelectric, and electro-optic properties and their functional perovskite structure. Typical examples include lead titanate ($PbTiO_3$ [PT]), lead zirconate ($PbZrO_3$ [PZ]), and lead zirconium tianate (Pb (Zr_xTi_{1-x})O_3 [PZT]), lithium niobate ($LiNbO_3$), zinc oxide (ZnO) etc. In recent years, polycrystalline aluminum nitride (A1N) has become an important ceramic material used in substrates for hybrid microelectronics. Although AlN exhibits no piezoelectric activity in the bulk form, AIN thin films exhibit piezoelectric properties when properly oriented on a compatible substrate. Moreover, its high-temperature piezoelectric response is the most attractive property for practical applications. For comparison, **Table 1** lists the piezoelectric properties and CTE values of promising candidates for the piezoelectric thin film sensor, including PZT, $LiNbO_3$, AlN, and ZnO [29,30,31,32,33].

Table 1 Comparison of piezoelectric materials

Figure of Merits	PZT	AlN	ZnO	LiNbO$_3$
Current response: ($\varepsilon_{31,f}$) [C/m^2]	-14.7	-1.0	-0.7	-5.8
Voltage response: ($\varepsilon_{31,f}/\varepsilon_o\varepsilon_{33}$) [GV/m^{-1}]	-1.2	-10.3	-7.2	N/A
Coupling Coefficient (k$_{p,f}$)^2 on Si	0.2	0.11	0.06	0.02
Curie Temperature T$_c$ (°C)	~300	~1100	N/A	1210
CTE □ (×10^{-6} K^{-1})	7.2	4	5	11
Electrical Resistivity (Ω.cm)	10^9	10^{11}-10^{16}	10^8	10^{11}

Note: CTE α (×10^{-6} K^{-1}): 13 for H13 steel, 6 for Al$_2$O$_3$, 6.5 for TiAlN, and 10.1 for Ti.

Materials were selected based on their high temperature stability, good piezoelectric property and compatibility with the host structure. It is evident from the Table 1 that only materials with a high Curie temperature such as AlN and LiNbO$_3$ would be applicable for piezoelectric measurements at elevated temperatures (e.g. up to 700°C in Al pressure die-casting and in excess of 700°C for aerospace applications). AlN has high thermal conductivity and is a non-ferroelectric piezoelectric material with good mechanical, thermal and chemical stability. The electrical band gap of stoichiometric AlN is high (6.2 eV), which indicates that the piezoelectric signal would prevail over the DC leakage through an extended period. AlN exhibits a high electrical resistivity (10^{16} Ω.cm) which leads to its high resistance to electrical breakdown and charge leakage. Therefore, considering the combined value of high thermal stability, high Curie temperature (~1100 °C), high electrical resistivity, high thermal conductivity and good piezoelectric response, an AlN thin film is an excellent piezoelectric candidate to use at elevated temperatures. Being covalently bonded, this material will not introduce any ionic conduction, and due to the large band gap, the electronic conduction at high temperature will remain minimal. AlN crystallizes in a hexagonal crystal structure. The Al atoms and N atoms are placed on alternate planes in a hexagonal array as shown in **Figure 7** [34].
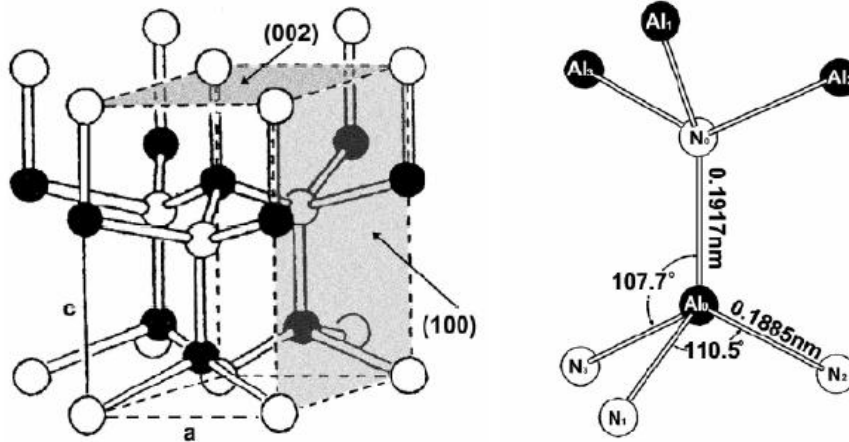
Figure 7 Wurtzite Structure of Aluminium Nitride [34]

The ultimate piezoelectric activity in this material is found to be restricted to the perpendicular direction to the hexagonal arrays or (002) orientation, also known as the 'c'-axis [35,36]. It also happens to be the natural (thermodynamically/energetically stable) growth direction of a thin film. The hexagonal planes have a low surface energy (due to the close packed geometry in which most of the chemical bonds are saturated, and there are no dangling bonds). Due to this low energy, an AlN crystal will tend to have these planes (002) exposed, which means a flake like shape will be the lowest energy configuration of an AlN crystal. The high mechanical bonding might prevail against the thermal stress developed at the interface (between the sensor element and the substrate) due to this difference.

2.6 Project Goals and Objectives

The primary objective of this project is the development of an optimized surface engineering coating system contains a CrN/AlN nanoscale multilayer layer and an AlN piezoelectric thin film sensor.

The project consisted of four major parts:

1. First goal is the development of the optimized multifunctional tribological outer layer that exhibits super hardness, good toughness, good adhesion and thermal stability. This task includes a compositionally graded CrAlN layer design and the CrN/AlN superlattice design.

2. The second goal is the design and development of the AlN based thin films, which has been identified as a good candidate for the thin film sensor material. This task includes the optimization of the deposition conditions for obtaining highly (0002) oriented AlN thin film sensor material. Validate the high temperature thermal stability of the AlN thin film sensor

16

materials.

3. Third goal is the evaluation of coated small die components in the industry in-plant trials.

4. The last goal is the technical transfer of the developed coating system from laboratory scale to industrial facilities. We have been working closely with Phygen Inc. in the last two years for the technical transfer. The optimized coating system has been successfully reproduced in the industrial coater.

2.7 Planned Approaches

2.7.1 Deposition Technique

Pulsed closed field unbalanced magnetron sputtering has been selected as the coating deposition technique. Magnetron sputtering is a method of deposition where plasma consisting of partially ionized Ar^+ accelerates the inert ions toward a target material. The target material is then ejected from its solid state, creating a material plume, which is attracted to the substrate [37]. Magnetron sputtering aids this process by using magnetic field lines to direct/focus the ions (**Figure 8**). The ion current (density of ionized atoms hitting the target) is increased by an order of magnitude over conventional diode sputtering systems, resulting in faster deposition rates at lower pressure. The lower pressure in the chamber also helps create a cleaner film, and a lower target temperature enhancing the deposition of high quality films.
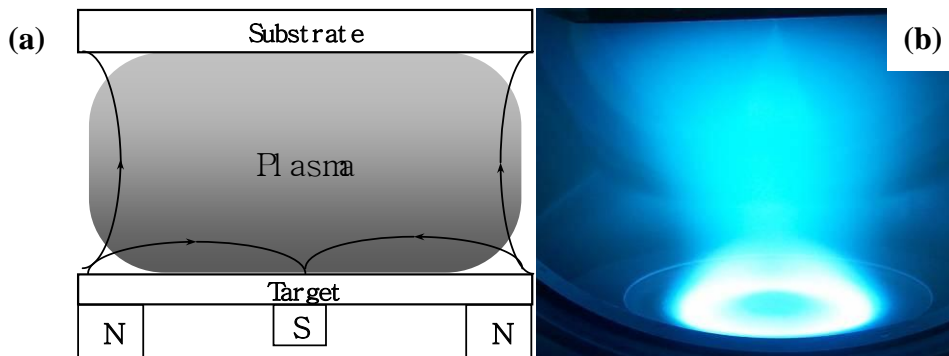
Figure 8 The magnetic configuration and plasma confinement in(a) unbalanced magnetron sputtering, and (b) A dc glow discharge generated in unbalanced magnetron sputtering

Closed field unbalanced magnetron sputtering (CFUBMS) is a special designed magnetron sputtering technique. The purpose of CFUBMS is to enhance ionization and increase the ion current density in magnetron sputtering as proposed by Sproul et al [38,39] and Tominaga [40]. The ion current density can be further increased to 5-20 mA/cm^2 compared to the traditional magnetron sputtering (2-10 mA/cm^2). A schematic and a photo of the PCFUBMS

system at the CSM are shown in **Figure 9**. The major feature in the CFUBMS system was the idea of using unbalanced magnetrons in an arrangement whereby neighboring magnetrons are of opposite magnetic polarity. Using this arrangement, the deposition zone in which the substrates are located is surrounded by linking magnetic field lines (**Figure 9a**). This traps the plasma region, prevents loss of ionizing electrons escaping to the chamber walls resulting in much higher plasma density (ion current densities) and dense, hard well adhered coatings by enhanced chemical reaction at the substrate. **Figure 9b** shows the CFUBMS deposition system used for the research work.
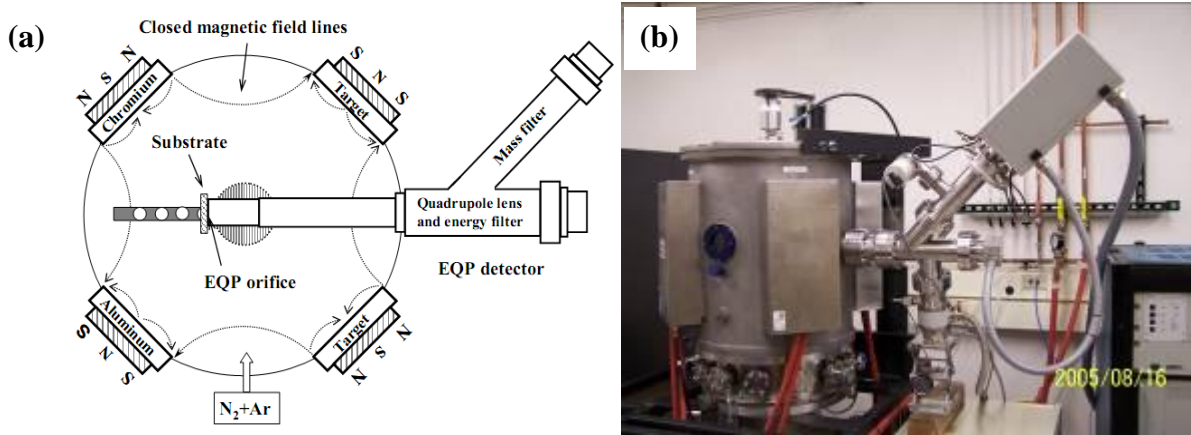
Figure 9 Closed field unbalanced magnetron sputtering configuration

2.7.2 Experimental and Characterization Techniques

2.7.2.1 The coating depositions

All coating were deposited by the pulsed CFUBMS system. The CFUBMS system is equipped with four unbalanced electrodes/targets uniformly positioned at 90-degree intervals in a closed field configuration around the cylindrical deposition chamber. Pure chromium and aluminum targets (99.99%) (both targets are 298×106 mm^2 in size) were driven by an Advanced Energy Pinnacle-plus power supply and were sputtered in the nitrogen and argon atmosphere to reactively produce the coating systems. The substrates were placed along the middle line between chromium and aluminum targets and was facing to the chamber wall midway between the chromium and aluminum targets. The distance from the substrate to the chamber wall midway between the chromium and aluminum targets was kept at 203 mm.

For all coating depositions, the chamber was evacuated to pressure below 1.33×10^{-5} Pa using a pumping unit consisting of a rotary pump and a cryo pump before the coating deposition. The working pressure and gas flow rate were controlled by MKS flow meters and a throttling

value together with a MKS 146C control system. The substrates were sputter etched in an argon plasma at a 1.02 Pa working pressure with a bias of -400 V for 30 minutes to remove the surface contaminants prior to all film depositions. A -50 V substrate bias was applied during all film depositions. The working pressure during coating depositions was kept constant at 0.27 Pa. The substrate temperature was approximately 473 K resulting from the bombarding species only.

1) The compositionally graded CrAlN coating depositions

The compositionally graded coating architecture contains three different layers. The first layer was a thin chromium adhesion layer (the layer thickness is of about 60-100 nm) used to improve the adhesion between the substrates and the above coating layers. It was deposited in pure argon with a chromium target power of 1000 W. Then a Cr_xN_y layer (the layer thickness is of about 150 nm) with increased nitrogen content from bottom to top (max. 50 atomic %) was deposited on the chromium layer by increasing the nitrogen to argon flow ratio from 40:60 to 70:30 in the chamber. The third layer was the compositionally graded $Cr_{1-x}Al_xN$ layer deposited by gradually incorporating aluminum into the Cr_xN_y binary phase. The increase of aluminum concentration in the graded $Cr_{1-x}Al_xN$ layer is defined by the power law equation:

$$\frac{Al}{(Cr + Al)}\% = 58\% \times \left(\frac{k}{L}\right)^p$$

Where the right side of the equation is the aluminum concentration in the film, 58 at % is the maximum aluminum content that will be achieved on the top of the graded $Cr_{1-x}Al_xN$ layer, k is the distance in the graded $Cr_{1-x}Al_xN$ layer from the bottom Cr_xN_y layer, L is the total thickness of the $Cr_{1-x}Al_xN$ graded region, which is about 1.2~1.5 µm and p is the exponent that defines the nature of the graded region.

The variation of the aluminum concentration in the graded $Cr_{1-x}Al_xN$ layer was achieved by fixing chromium target power at 200 W and varying the aluminum target power (100~800 W) as a function of k/L in the power low equation. Three power law scenarios have been used to vary the aluminum concentrations in the graded $Cr_{1-x}Al_xN$ layer, as shown in **Figure 10**:

1). When p=1, the aluminum concentration in the graded region is linear to k/L (red line)

2). When p=0.2, the $Cr_{1-x}Al_xN$ layer is an aluminum rich graded region (Black line)

3). When p=2, the $Cr_{1-x}Al_xN$ layer is a chromium rich graded region (Blue line)

The equation shown in the figure:

$$\frac{Al}{(Cr+Al)}\% = 58\% \times \left(\frac{k}{L}\right)^{p}$$
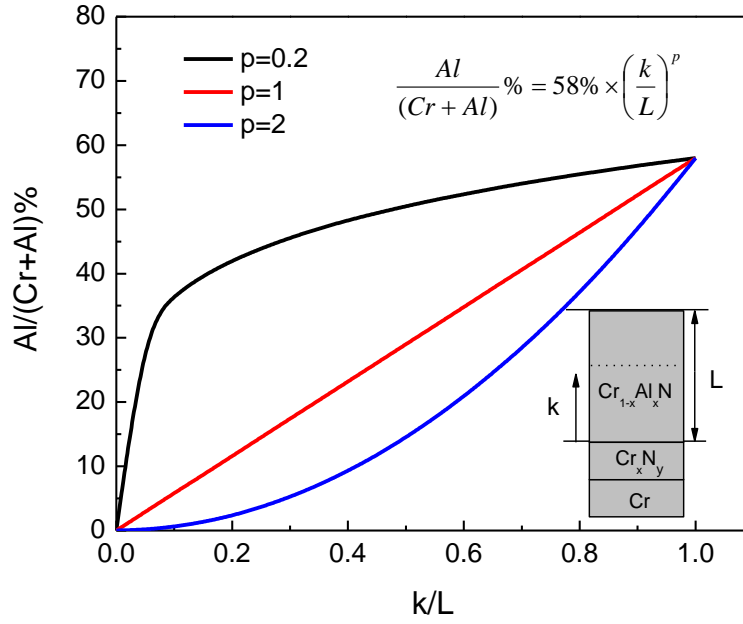
Figure 10 Aluminum concentration as a function of the graded region normalized distance with different power law scenarios.

2) The nanometer scale CrN/AlN superlattice coating depositions

The nanometer scale CrN/AlN superlattice coatings were deposited by sputtering one Cr and Al targets in the CFUBMS system. A 100 nm Cr and a 300 nm graded CrNx adhesion layers were firstly deposited on the substrates to improve the adhesion. CrN/AlN superlattice coatings with thickness of 2.0-2.7 µm were deposited by alternately depositing CrN and AlN nanolayers using a rotation device driving the substrate holder rotation back and forth between the Cr and Al targets. The Cr and Al targets were powered at 2.2 and 6.7 Wcm^{-2} respectively and pulsed at 100 kHz and 90% duty cycle asynchronously using an Advanced Energy Pinnacle Plus Power supply. The bilayer periods of the coatings were controlled by the settle periods of the substrate holder in front of the targets. A working pressure of 0.27 Pa, a nitrogen flow rate of 12 sccm (50% of the total flow) and a -60 V dc substrate bias were applied for all depositions.

3) The AlN piezoelectric coating depositions

The AlN piezoelectric thin films were also deposited in the CFUBMS system using a metal Al target (99.95%) in a gas mixture of high purity (99.999%) Ar and N$_2$. The Al source was powered using an Advanced Energy Pinnacle Plus Power supply, which can be operated in middle frequency pulse regions. During the positive pulse period, the target voltage is reversed to 10 percent of its nominal negative sputtering voltage in order to minimize the negative charge accumulation on the target and avoid target poisoning. Different Cr, Pt, Mo and Ti/TiN layers

were deposited as the bottom seed layer/electrode, which also acts as an adhesion layer in our coating system.

<u>2.7.2.2 The coating characterization techniques</u>

The average film thickness was measured using a Dektec 3030 profilometer. The texture and crystal structure of the films was characterized by grazing incident X-ray diffraction (GIXRD) at a 2-degree incident angle with a Siemens X-ray diffractometer (Model KRISTALLOFLEX-810) using Cu K_α radiation (20 kV, 30 mA). The residual stress of the films was determined by $\sin^2\psi$ method using the same X-ray diffractometer [41,42]. The AlN film texture was analyzed using XRD Rocking Curve method with a Simens X-ray diffractometer (model KRISTALLOFLEX-810). The composition and bonding nature of these films were analyzed by high-resolution x-ray photoelectron spectroscopy (XPS).

Characterization of the elemental chemical distributions in the $Cr/Cr_xN_y/Cr_{1-x}Al_XN$ graded films was carried out using a LECO 850A glow discharge optical emission spectrometry (GDOES). The coating microstructure was characterized on the fractured cross-section of the coatings deposited on the silicon wafer using a JSM-7000F field-emission scanning electron microscope (FESEM). A Philips/FEI CM200 transmission electron microscope (TEM) operated at 200 kV was used to examine the film cross-sectional microstructure and grain size.

The nanoindentation hardness and Young's modulus of the films were measured by a MTS Nano Indenter XP system. In order to avoid the substrate effect, the maximum indentation depth was set at 10% of the film thickness. Sixteen measurements separated by a distance of 60 µm were measured for each sample to obtain the mean value and the standard deviation. The scratch tests were carried out using a commercial scratch tester Teer ST2200. A Rockwell C diamond stylus (cone apex angle 120°, tip radius R=0.2 mm) was used to perform the tests. The applied load on the stylus was linearly increased from 2.3 N (the weight of stylus itself) up to 70 N with a constant loading rate of 100 N/min. The wear resistance experiments were carried out using a ball-on-disc (CETR) micro-tribometer in ambient atmosphere (relative humidity of 22±5 RH% and temperature of around 25 °C). The tests were performed at a normal load of 3 N against a WC–6% Co ball with a diameter of 1 mm. The sliding linear speed, the radius of wear track and total sliding distance were fixed at values of 20 mm/sec, 4.5 mm and 100 m, respectively. After the wear tests, the wear tracks were examined using a Veco 3D surface profilometer to measure the wear volume and calculate the wear rate.

The dynamic oxidation studies of AlN films were carried out in the differential scanning calorimetry (DSC) in which the AlN films deposited on a Si wafer was placed in the alumina crucible and were heated from room temperature to 1400 °C in flowing argon (55 sccm) using a heating rate of 20 Kmin^{-1}. An empty pure alumina crucible served as an inert reference. After the DSC tests, XRD measurements of the annealed films were carried out on a Philips X-ray diffractometer in the $\theta/2\theta$ geometry using Cu Kα radiation (20 kV and 30 mA) on order to investigate the phase transformations and structure evolution during heating procedure.

All of the previous methods that we have used to measure the piezoelectric response were only applicable at room temperature. However, we need to measure the piezo-response of our films at high temperatures. One proposed idea is to use a non-contact (remote) method such as a laser beam to shine at the system of the AlN thin film sandwiched between two electrodes, and then with the application of cyclic voltage, one can measure the displacement variation within the piezoelectric AlN thin film. A Michelson interferometer was used in this proposed measurement technique in collaboration with CSM physics department. In this setup, shown in **Figure 11**; a light source such as a laser source emits an electromagnetic wave, which is then divided at a half-transparent mirror into two beams with equal intensities. These beams are reflected back at two plane mirrors, one mirror is fixed and the other mirror is our sample, which will change dimensions upon voltage application, and return to the half-transparent mirror, where they are combined before they emerge at the screen or detector. The different paths may be of different lengths or be composed of different materials to create alternating interference fringes on a back detector.

By applying a voltage difference across the top and bottom electrodes in the AlN thin film system, one can measure the displacement change very precisely (in the order of pico-meter) due to piezoelectric effect by using the mentioned Interferometer setup.
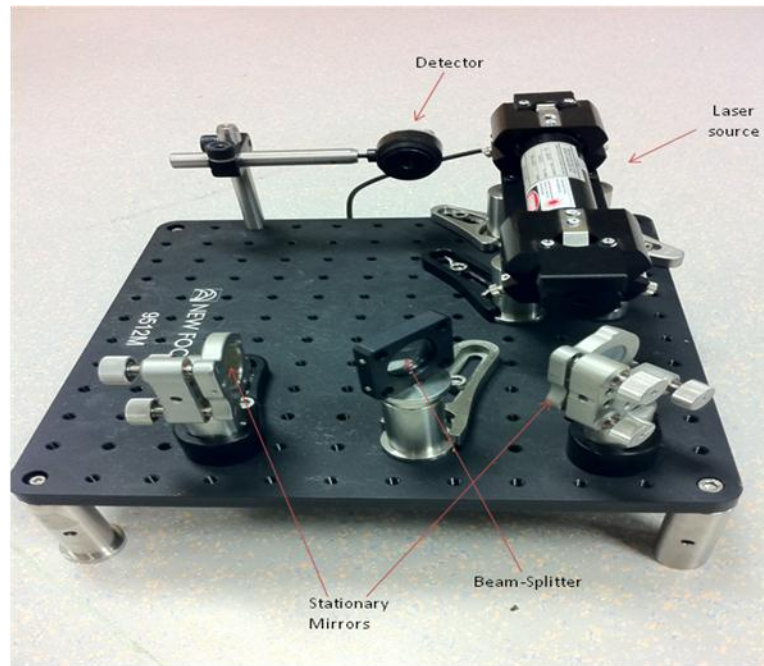
Figure 11. Schematic representation of a Michelson Interferometer

3. Results and Discussion

3.1 Optimization of a Compositionally Graded Multi-layer Coating System

3.1.1 X-Ray Diffraction Patterns

The GIXRD patterns of homogeneous and three compositionally graded $Cr/Cr_xN_y/Cr_{1-x}Al_xN$ coatings are presented in **Figure 12**. The homogeneous Cr-Al-N coating exhibit a B1 NaCl structure with (111), (200) and (220) reflections and the (200) reflection exhibits the highest intensity. In the graded coatings, the main peaks from B1 NaCl structure are still clearly observed. However, small fractions of Cr_2N peaks were revealed in the graded coating XRD spectra. The small amount of Cr_2N phase is possibly formed at the beginning of the graded Cr_xN_y layer at which the nitrogen to argon flow ratio is low during the deposition. Another important feature revealed in all graded coating XRD spectra is that there are no hexagonal AlN phases being observed.
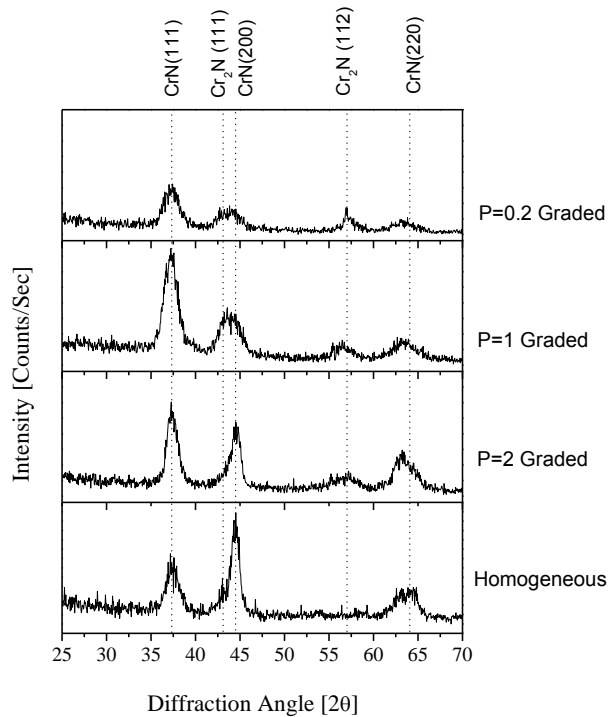
Figure 12 GIXRD spectra of homogeneous CrAlN and graded $Cr/Cr_xN_y/ Cr_{1-x}Al_xN$ coatings

3.1.2 GDOES Depth Profiles of the Graded Coatings

Figure 13 shows the GDOES depth profiles of the homogeneous and graded $Cr/Cr_xN_y/Cr_{1-x}Al_xN$ coating systems with the composition profiles in the $Cr_{1-x}Al_xN$ layer for p=2 (the $Cr_{1-x}Al_xN$ layer is a chromium rich graded region) and p=0.2 (the $Cr_{1-x}Al_xN$ layer is an

aluminum rich graded region), respectively. Five elements: chromium, aluminum, nitrogen, oxygen, and iron were chosen for the depth profiling. The distribution of these species is revealed clearly, with sharply defined interfaces between the different layers (indicated by dotted lines).
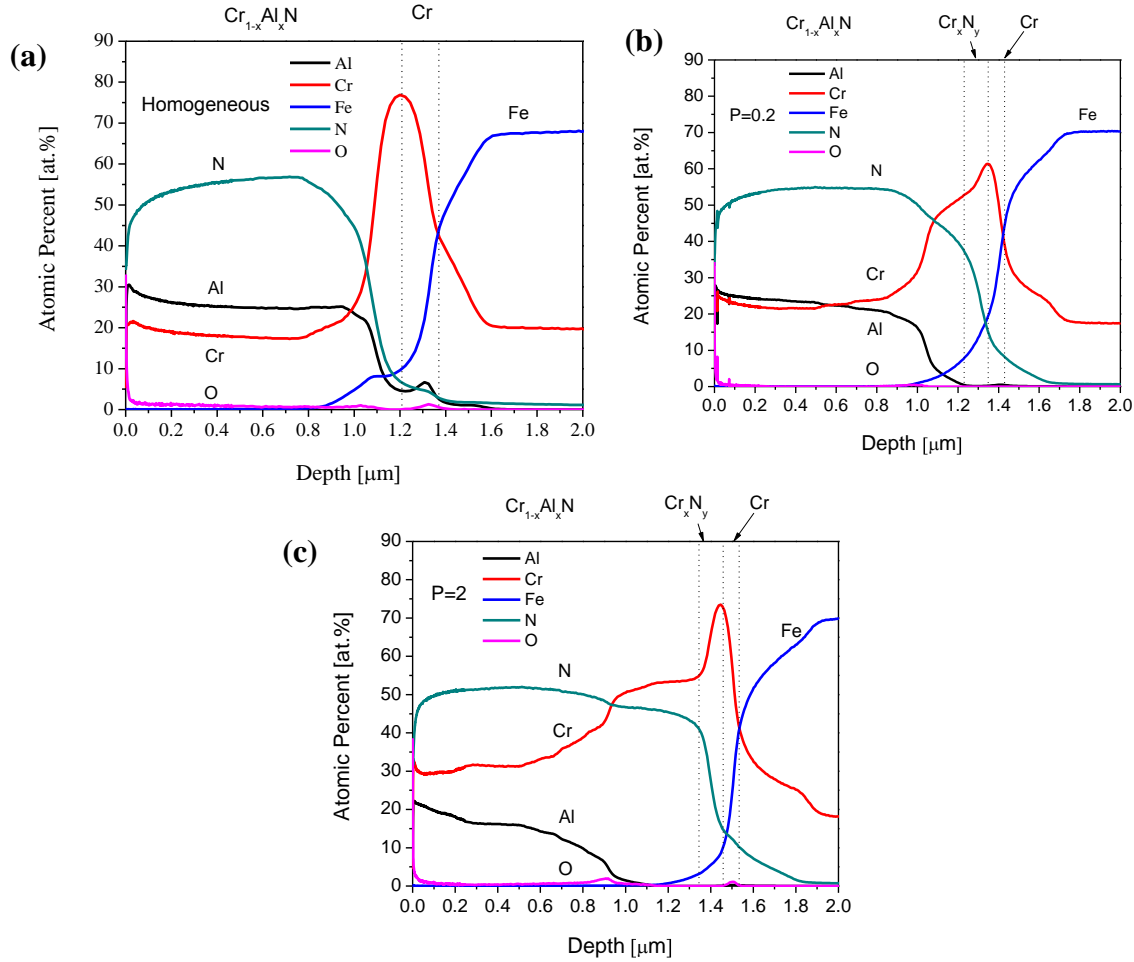
Figure 13 GDOES depth profile of (a) Homogeneous CrAlN coating, and Cr/Cr$_x$N$_y$/ Cr$_{1-x}$Al$_{lx}$N graded multiplayer coating structures with the composition profile in Cr$_{1-x}$Al$_x$N layer for (b) p=0.2 and (c) p=2.

The chemical depth profile of the homogeneous Cr$_{1-x}$Al$_{lx}$N coating is presented in **Figure 13a**. The GDOES profile shows that the homogeneous coating approximately contains 26 at.% aluminum and 18 at.% chromium, 54 at.% nitrogen and a small content of oxygen (less than 2~3 at.%). The chemical depth profiles of two compositionally graded Cr/Cr$_x$N$_y$/Cr$_{1-x}$Al$_x$N coatings (p=0.2 and p=2) are presented in **Figure 13b** and **13c** respectively. Three different layers can be identified. The chromium adhesion layer with 150 nm thickness was clearly observed above the substrate in both coatings. It is evident that a small amount of iron (from the substrate) and

nitrogen (from the Cr_xN_y layer) are diffused into the chromium adhesion layer, indicating increased interface bonding between the substrate, the chromium adhesion layer and the Cr_xN_y layer. Additionally, since the AISI 304 stainless steel substrate has 18-20 % of chromium, the chromium signal starts with a certain value (of about 18%).

The graded Cr_xN_y layer was deposited by varying the nitrogen to argon flow ratio from 40:60 to 70:30 at a constant working pressure (0.26 Pa) above the chromium layer. As a result, the nitrogen content in the Cr_xN_y layer increased from the bottom to the top in the layer, and thus the chromium content decreased correspondently. The stoichiometry near the interface between the Cr_xN_y layer and the $Cr_{1-x}Al_xN$ layer was found from GDOES to be $Cr_{0.48}N_{0.52}$ with a small amount of oxygen in both coatings.

However, the depth profiles of $Cr_{1-x}Al_xN$ graded layers in these two coatings exhibit significant difference. When the $Cr_{1-x}Al_xN$ layer is an aluminum rich graded region (p= 0.2) (**Figure 13b**), it was found that the aluminum content (black curve) increased rapidly in the first 200 nm to nearly 20 at.%, and then gradually increased to 27 at.% near the surface of the coating, while the chromium content decreased correspondingly. The nitrogen content in p=0.2 graded $Cr_{1-x}Al_xN$ layer was almost constant at 54 at.%. On the other hand, when the $Cr_{1-x}Al_xN$ layer was deposited with a chromium rich graded region (p= 2) (**Figure 13c**), the graded layer showed a depletion of aluminum but enrichment in chromium, in that the chromium remained high concentration in the first 200 nm thickness, while the aluminum is hardly to be observed due to the low aluminum target power (100 W) used at the beginning in this coating. Although the aluminum concentration was observed to increase after the first 200 nm, the increase rate is much less than in the p=0.2 graded coating. Overall, the coating depth profiles presented in **Figures 13b and 13c** confirmed that the graded coating architectures are in accordance with the grading scenarios shown in **Figure 10**.

3.1.3 Microstructure of Homogenous and Graded CrAlN Coatings

Figure 14 provides a bright field TEM micrograph and corresponding selected area electron diffraction (SAED) pattern obtained from the homogeneous Cr-Al-N film. The film exhibits a dense columnar structure. The SAED pattern showed that the Cr-Al-N film was poly-crystalline with a FCC Cr-Al-N structure containing (111), (200) and (220) reflections. From d-spacing measurements of the diffraction spots, the lattice constant of this film was calculated to be 0.411 nm, which is less than that of the standard FCC-CrN (a=0.414 nm), indicating a

contracted lattice compared to that of FCC-CrN due to the smaller sized aluminum atoms occupying the chromium lattice sites. The continuous and diffuse ring segments indicate that the film consists of small grains, in the nano-scale range. The dark field image in **Figure 14b** was obtained using the circled portion of the (200) ring segment along the film growth direction marked in **Figure 14a**. The dark field image confirmed that the columnar grain size is in the nano-scale, in which the bright regions (columns) represent the existence of the grains attributed to the selected orientation. It can be seen that the bright columns in the (200) orientation have an average grain size of 20-40 nm. The dark field images confirmed that the Cr-Al-N film exhibits a polycrystalline structure containing nanostructured columnar grains.
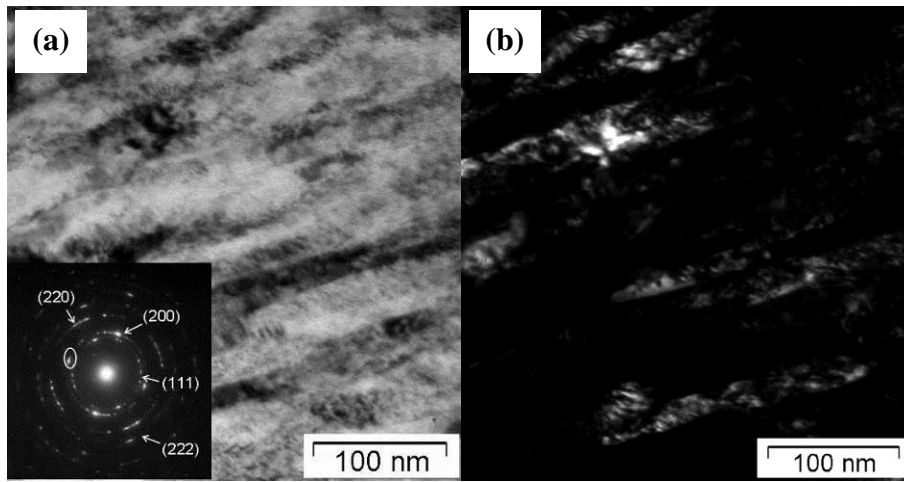
Figure 14 (a) a bright field TEM micrograph and corresponding SAED pattern obtained from the homogenous CrAlN coating, (b) dark field TEM micrographs imaged using (200) diffraction rings indicated by circles in the (a).

Figures **15a** and **15b** show the comparison of the cross-sectional FESEM micrographs and EDS elemental mapping of the $Cr/Cr_xN_y/Cr_{1-x}Al_xN$ multilayer coatings with the composition profiles in $Cr_{1-x}Al_xN$ layer for p=2 and p=0.2 respectively.

From the EDS elemental mapping, the nitrogen distribution is homogeneous in both coatings (see the red mapping in **Figures 15a** and **15b**). However, the chromium and aluminum elemental distributions are quite different. The $Cr_{1-x}Al_xN$ layer with a p=2 composition profile began with a chromium rich and aluminum deficient region in which a large size columnar structure (80-100 nm) is developed. As the aluminum concentration was increased near the top of the $Cr_{1-x}Al_xN$ layer, the columnar grain size decreased and the structure becomes more dense (**Figure 15a**).

On the other hand, the $Cr_{1-x}Al_xN$ layer with a p=0.2 composition profile began with a high Al concentration. The aluminum content was slightly increased up to near 58 at.% from the bottom to the top. As a result, the composition difference throughout the graded zone is small, thereby forming a consistent columnar structure with the columnar size of about 60-70 nm (**Figure 15b**).
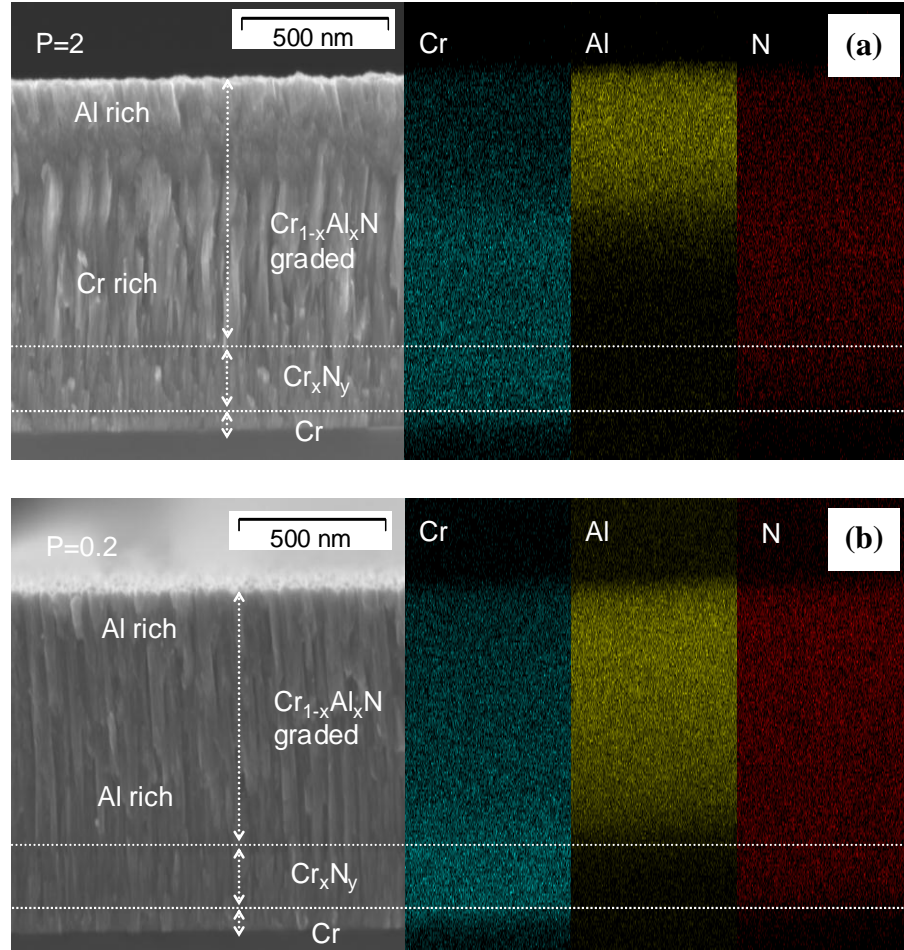
Figure 15 The cross-sectional FESEM micrographs and EDS elemental mapping of the Cr/Cr_xN_y/ $Cr_{1-x}Al_xN$ multiplayer coatings with the composition profile in Cr1-xAlxN layer for (a) p=2 (Cr rich graded region) and (b) p=0.2 (Al rich graded region)

3.1.4 Mechanical and Tribological Properties

Table 2 summaries the mechanical and tribological properties of graded Cr/Cr_xN_y/$Cr_{1-x}Al_xN$ multilayer coatings with the composition profiles in $Cr_{1-x}Al_xN$ layer of p=2, p=1, and p=0.2. The properties of homogeneous $Cr_{1-x}Al_xN$ single layer film (x=0.585) are also present in the table for comparison.

Table 2 Summary of Mechanical and Tribological Properties of Cr/Cr$_x$N$_y$/Cr$_{1-x}$Al$_x$N Multilayer Coatings

Properties	Homogeneous	P=2	P=1	P=0.2
Film Thickness [μm]	1.2	1.6	1.2	1.5
Hardness (H) [GPa]	36.38±3.98	24.65±2.98	28.1±2.56	34.61±3.22
Young's Modulus (E) [GPa]	369.9±29.3	272.7±28.6	316.23±30.51	378.47±24.72
H/E	0.0984	0.090	0.088	0.091
L$_c$ [N]	28	36	35	42
Residual Stress [GPa]	-4.8	-1.78	-1.54	-2.25
Coefficient of Friction	0.38	0.60	0.56	0.45
Wear Rate (W$_N$) [10^{-6}mm^{3}N^{-1}m^{-1}]	2.87	4.32	3.78	3.12

As can been seen, the homogeneous films and the graded coatings at p=0.2 exhibit high hardness values of 36 and 34 GPa respectively, while the graded coatings at p=2 and p=1 have relatively low hardness values of 24 and 28 GPa respectively. The low hardness in the graded coatings (p=2 and 1) may be attributed to the wide low aluminum concentration graded zone. The graded zone near the coating surface with a high aluminum concentration showed a denser structure which may have a much higher hardness value than that of the graded zone near the interface between the Cr$_{1-x}$Al$_x$N and Cr$_x$N$_y$ layers as shown in **Figure 15a**. As a result, during the nanoindentation test, when the indenter tip penetrates the very surface and moves deeper into the coating, the softer subsurface region may not give enough support to the top hard region, suggesting a lower overall hardness for the graded coatings at p=1 and 2. On the other hand, when the grading profile is at p=0.2, the composition and structure difference in the graded zone is small, which is helpful to maintain the higher hardness on the top. Nevertheless, all the graded films exhibit much lower residual stress than the homogeneous Cr$_{1-x}$Al$_x$N (x=0.585) film by means of relaxation of the stress throughout the graded zone (**Table 2**).

Experimental results show that the adhesion strength between the substrate and graded multilayer coatings is better than that of homogeneous Cr$_{1-x}$Al$_x$N (x=0.585) films. When p=0.2, the multilayer coating withstood a 42 N load without significant coating failure. **Figure 16** shows the comparison of optical microscope images of scratch tracks for the homogeneous Cr$_{1-x}$Al$_x$N (x=0.585) coating and a Cr/Cr$_x$N$_y$/Cr$_{1-x}$Al$_x$N graded coating (p=0.2). For the homogeneous single coating, the microstructure and the properties of the film are completely different from the

underlying substrate. This situation causes the accumulation of stress at the interface between the substrate and the film during deformation, which will cause the cracking and delamination of the coating from the substrate easily. Extensive cracks were developed inside the scratch track and film delamination was found at 28 N normal loads, see **Figure 16a**. On the other hand, in the graded coating (p=0.2), the stress cannot concentrate any longer in the boundary and is distributed in the graded zone during deformation. The increased number of interfaces in the graded coatings acting as obstacles for dislocation movement can also control crack propagation directions, thereby increasing coating capacity for energy dissipation before losing substrate protection. This graded architecture provides a system in which microcracks are very difficult to form and propagate and the adhesion strength can be improved (**Figure 16b**). Another possibility is that the chromium content gradually decreased from the chromium adhesion layer to the Cr_xN_y graded region and then to the $Cr_{1-x}Al_xN$ layer in the multilayer coatings effectively increasing the interface bonding energy, thereby also increasing the coating adhesion strength. **Figure 16b** shows that no coating delamination was observed along the scratch track until the normal load was increased to 42 N and very little conformal cracks were formed inside the track for the graded film indicating good film toughness.
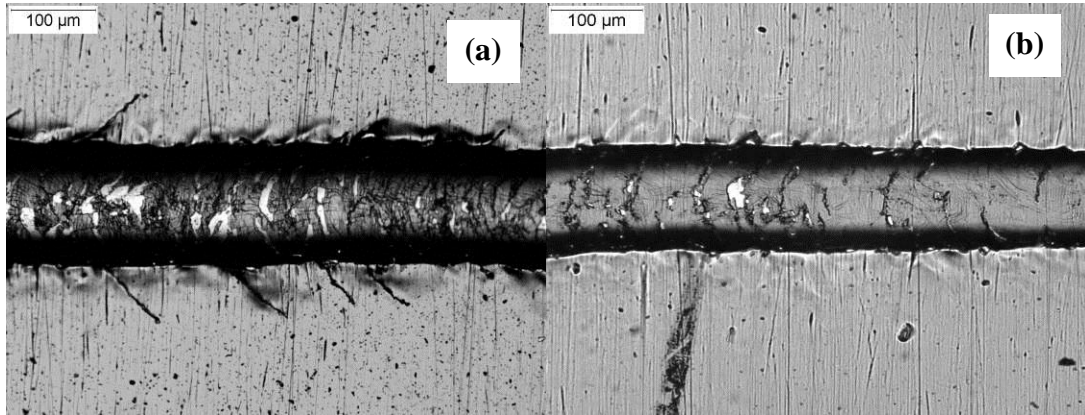
Figure 16 Scratch test track morphologies for (a) Homogeneous CrAlN film and (b) Cr/Cr$_x$N$_y$/ Cr$_{1-x}$Al$_x$N graded coating (p=0.2)

The coefficient of friction (COF) values of the homogeneous and graded $Cr_{1-x}Al_xN$ coatings are presented in Table 2 and the corresponding wear track morphologies after sliding against 1 mm WC ball at a normal load of 3 N for 100 meters sliding length are shown in **Figure 17**. The homogeneous $Cr_{1-x}Al_xN$ film exhibited a low COF value of 0.37 and a low wear rate of $2.87 \times 10^{-6} mm^3 N^{-1} m^{-1}$, indicating excellent wear resistance in the homogeneous films. The excellent wear resistance performance in the homogeneous films may be related to the high film

hardness and dense structure.

In the cases of graded coatings, the COF, as shown in Table 2, varied from 0.45 to 0.6. From **Figures 17b** to **17d**, the graded coatings show different degrees of wear. When p=2, the wear track exhibited extensive abrasive wear and EDS analysis inside the track revealed the presence of substrate material (**Figure 17b**). Hence the high COF and severe wear in this coating is due to the contact of the substrate material with the WC ball with rapid wear attributable to its lower hardness. As the hardness increased in other two graded coatings, the COF and the wear damage in the wear track decreased correspondingly. When p=0.2, the graded coating has a COF value of 0.45 with some abrasive wear along the wear track edge (**Figure 17d**).
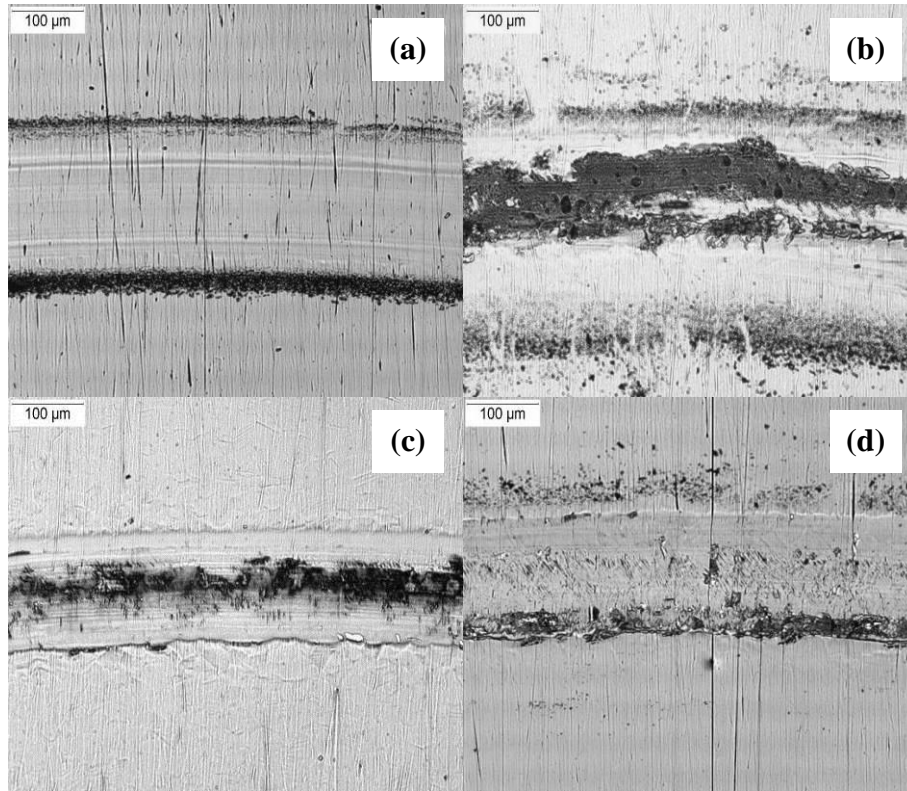
Figure 17 Wear track optical micrographs of homogeneous CrAlN film and Cr/CrxNy/Cr1-xAlxN multilayer coatings after sliding against 1 mm WC ball at a load of 3 N for 100 meters sliding length: (a) Homogeneous coating, (b) p=2, (c) p=1, and (d) p=0.2

From the above mechanical and tribological properties study, it was found that the graded structure can effectively decrease the residual stress in the film and will also increase the film adhesion properties compared with those properties of homogeneous films. The Cr-Cr_xN_y graded zone between the substrate and the $Cr_{1-x}Al_xN$ graded layer may contribute to adhesion improvement. It is expected that the proposed optimized die coating architecture should have

improved thermal fatigue resistance compared to the single layer homogeneous $Cr_{1-x}Al_xN$ coatings [43]. However, the results also demonstrate that different compositional grading architectures will have a significant influence on the coating hardness and wear resistance. In this study, the graded coating with an aluminum rich graded region (p=0.2) exhibited high hardness (34 GPa), improved adhesion strength (L_c=42 N), and good wear resistance (COF=0.45) which could be used as one of the candidate coating systems for the engineered die casting coating architecture. Alternatively, the coatings could be subjected to controlled oxidation in air or oxygen at elevated temperature that is below the tempering temperature of H13 tool steel substrate. In another aspect, the deposition conditions for producing the graded multilayer coatings can further be optimized by incorporating the pulsed ion energy bombardment to increase the coating density and decrease the coating grain size [44,45].

3.1.5 Summary (I)

Nanostructured polycrystalline Cr-Al-N film and differently graded $Cr_{1-x}Al_xN/Cr_xN_y/Cr$ multilayer coating systems have been deposited using pulsed CFUBMS.

Three power law scenarios have been adopted to vary the Al concentration in the graded $Cr_{1-x}Al_xN$ layer: (i) p=1, the aluminum concentration was increased linearly in the $Cr_{1-x}Al_xN$ layer. (ii) p=0.2, the $Cr_{1-x}Al_xN$ layer is a aluminum-rich graded region, and (iii) p=2, the $Cr_{1-x}Al_xN$ layer is a chromium-rich graded region. It was found that all the graded films exhibit much lower residual stress than the homogeneous $Cr_{1-x}Al_xN$ (x=0.585) film by means of relaxation of the stress throughout the graded zone. The graded film also exhibited higher adhesion strength compared to that of the homogeneous film. The $Cr-Cr_xN_y$ graded zone between the substrate and the $Cr_{1-x}Al_xN$ graded layer may contribute to adhesion improvement. However, the different power law grading architectures have a significant influence on the film hardness and wear resistance, which is connected with the variation of the nanostructure in the $Cr_{1-x}Al_xN$ layer. When p=2 and p=1, the graded films exhibited relatively low hardness values (24 and 26 GPa respectively) and a high COF (0.55 to 0.60) due to a wide low aluminum concentration graded zone, which exhibit larger columnar grains and less dense structure compared to the top higher aluminum concentration zone. When p=0.2 the graded film exhibited both high hardness (34 GPa) and good wear resistance (COF=0.45) due to the structural consistency in the graded zone, in which a dense structure with typical columnar grain less than 40 nm was observed. The results demonstrate the importance of choosing proper compositional structure grading strategies

in achieving optimized structure and properties in a graded multilayer coating system.

3.2 Optimization of the Nanoscale Multilayer CrN/AlN Superlattice Coating System

3.2.1 Microstructure of CrN/AlN Superlattice Coatings

       Figure 18a shows the low angle XRD patterns of CrN/AlN coatings. The bilayer period (Λ) values of the coatings were calculated using the modified Bragg equation and summarized in **Table 3**. The CrN/AlN superlattice coatings with different Λ of 2.5 to 22.5 nm have been deposited. The diffraction peaks of all coatings exhibit good intensity, confirming their layered structure. However, the peak intensities decreased as the Λ is less than 3 nm, indicating a decreased interface sharpness. The composition analysis showed that the coatings have nitrogen concentration in the range of 44.5 to 48.3at.%. The Al/(Cr+Al) ratios of the coatings exhibit small variations from 61.5% to 66.5% (**Table 3**).

       Figure 18b shows the GIXRD patterns of CrN/AlN coatings with different Λ values obtained using a 2° incident angle. The coatings with Λ less than 4.7 nm exhibit a cubic NaCl-type structure, in which the (111), (200) and (220) reflections of face center cubic (fcc) CrN phase were observed, suggesting that the CrN layers epitaxially stabilize the AlN layers to NaCl-type structure when the Λ and the AlN layer thickness are small. As the Λ was increased to above 6.0 nm, broad diffraction peak centered at 35.8^o which belongs to the h-AlN (002) was revealed, indicating the AlN layers exhibit a Wurtzite structure as the AlN layer thickness was increased. Nevertheless the (200) and (220) diffraction peaks from the c-CrN layers remain present in all coatings. It is the AlN layer thickness that determines the epitaxial stabilization of NaCl-type AlN layers in the CrN/AlN coatings.
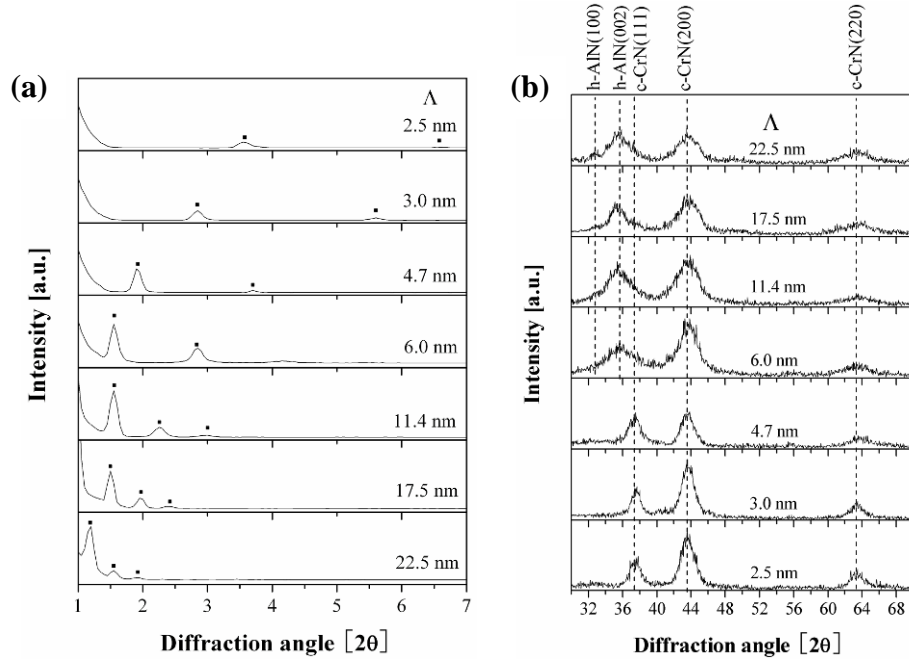
Figure 18 (a) LAXRD patterns and (b) GIXRD patterns of CrN/AlN superlattice coatings of different bilayer periods

Table 3 Chemical compositions, bilayer period (Λ) and the thickness of CrN/AlN coatings

Sample ID	Settle periods of the substrate in front of		Chemical compositions					Λ [nm]	Coating thickness [μm]
	Cr target [s]	Al target [s]	Cr [at.%]	Al [at.%]	N [at.%]	O [at.%]	Al/(Cr+Al)		
S1	1	5	19.4	30.8	47.4	2.4	61.5%	2.5	2.0
S2	2	10	19.5	31.7	45.5	3.3	62.0%	3.0	2.3
S3	3	15	16.9	32.5	47.9	2.7	65.8%	4.7	2.7
S4	4	20	19.3	33.1	44.5	3.1	63.2%	6.0	2.5
S5	10	50	17.5	31.9	48.3	2.3	64.7%	11.4	2.4
S6	16	80	18.5	34.5	45.4	1.6	65.1%	17.5	2.7
S7	20	100	16.6	32.9	47.3	3.2	66.5%	22.5	2.2

CrN/AlN coatings with Λ of 4.7 and 2.5 nm were examined using TEM. As shown in **Figure 19a**, the CrN (dark) and AlN (bright) layers alternating in growth direction with well-defined interfaces were observed. The SAED pattern as inserted in **Figure 19a** confirms a nano-scale polycrystalline structure corresponding to the single fcc phase, in which the (111), (200), (220) and (311) reflections were clearly shown. The Λ of the coating was found to be around 4.7 nm which is consistent with the LAXRD result. The thickness of the AlN layers was measured to be 3.3 nm, which is estimated to be the critical thickness for the epitaxial stabilization of NaCl-type AlN layers in the CrN/AlN coatings. When the Λ was decreased to 2.5 nm, the interfaces between the layers became less sharp due to the extremely low CrN layer thickness and the

possible inter-diffusion between the layers, as shown in **Figure 19b**.
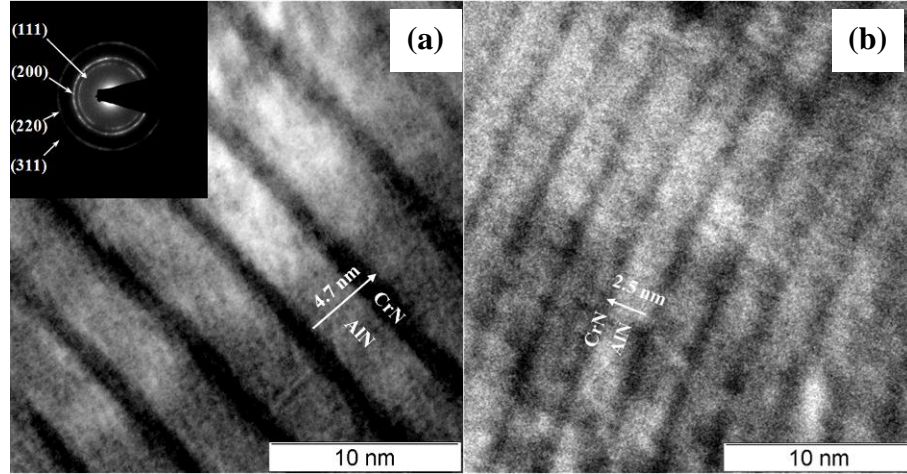
Figure 19 TEM micrographs of CrN/AlN superlattice coatings (a) Λ=4.7 nm and (b) Λ=2.5 nm

3.2.2 Properties of the CrN/AlN Superlattice Coatings

Figure 20 shows the hardness and Young's modulus of CrN/AlN coatings as a function of the Λ. The coatings exhibit high hardness above 35 GPa with Λ values from 2.5 to 4.7 nm, in which the AlN layers are in the NaCl-type structure. A super hardness of 45 GPa was achieved in the coating with a Λ of 3.0 nm and an Al/(Cr+Al) ratio of 62 at.%. This hardness is much higher than the single layered CrAlN (34-36 GPa) coatings which have similar Al/(Cr+Al) ratios [46] and CrN coatings (24GPa) deposited using the same P-CFUBMS deposition system at similar pulsing conditions [47].

The hardness enhancement can be explained by several aspects, e.g. the hindering of the dislocation movement, the Koehler's effect, and the coherency strain in the lattice mismatched materials [48,49]. In general, the dislocation blocking occurs when two layers in the multilayer have different shear moduli, and therefore different dislocation line energies. Dislocations prefer to remain within the layer with the lower shear modulus (CrN). An additional stress is required to move the dislocation into the layer with higher shear modulus (AlN) compared to the stress required to move the dislocation in a single layer coating with the homogeneous shear modulus. Additionally, the coherency strain between mismatched crystalline layers will also lead to the hardening. When the Λ is very low (less than 3 nm), the hardness of CrN/AlN coatings decreased to the range of 33~36 GPa, which are close to that of the single layer CrAlN coatings.

A significant decrease in the hardness to 23-25 GPa was identified in CrN/AlN coatings

when the bilayer period is larger than 6.0 nm, in which the AlN layers exhibit Wurtzite type structure (**Figure 18**). It should be noted that these hardness values are even less than the single layer c-CrAlN coatings of similar Al/(Cr+Al) ratios. It is suggested that the formation of Wurtzite type AlN layers as the AlN layer thickness was increased and an increase in the Λ together will lead to the rapid drop of the hardness of CrN/AlN coatings.
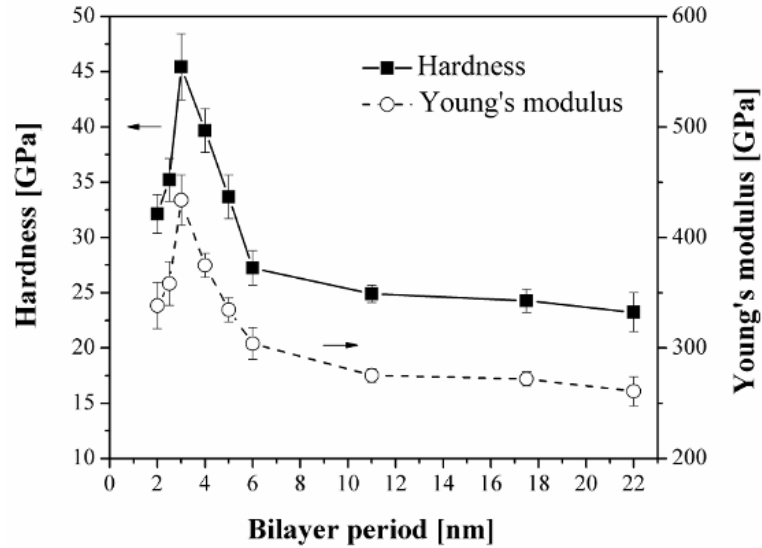
Figure 20 Nanoindentation hardness and Young's modulus of CrN/AlN superlattice coatings as a function of the bilayer period

Figure 21 shows the SEM micrographs of the indent morphologies after Rockwell C-Brale indentations of CrN/AlN coatings of different Λ values. The coatings containing Wurtzite type AlN layers (with large Λ of 22.5, 11.4 and 6.0 nm) exhibit poor adhesion and toughness. Almost all coatings along the indent boundary were delaminated in the Λ=22.5 nm coating, which can be associated with a poor HF6 adhesion strength quality [50]. The Λ=11.4 nm and Λ=6.0 nm coatings also exhibit massive delaminations of the coatings and cracks along the indent boundary, which can be associated with HF5 and HF4 adhesion strength qualities respectively. However, improved coating adhesion and toughness were identified in the coatings containing NaCl type AlN layers (with small Λ of 4.7, 3 and 2.5 nm). These three coatings show no cracks and very few delaminations along the indent circumference after the Rockwell-C indentation tests, indicating good toughness and adhesion (HF1 adhesion strength quality).
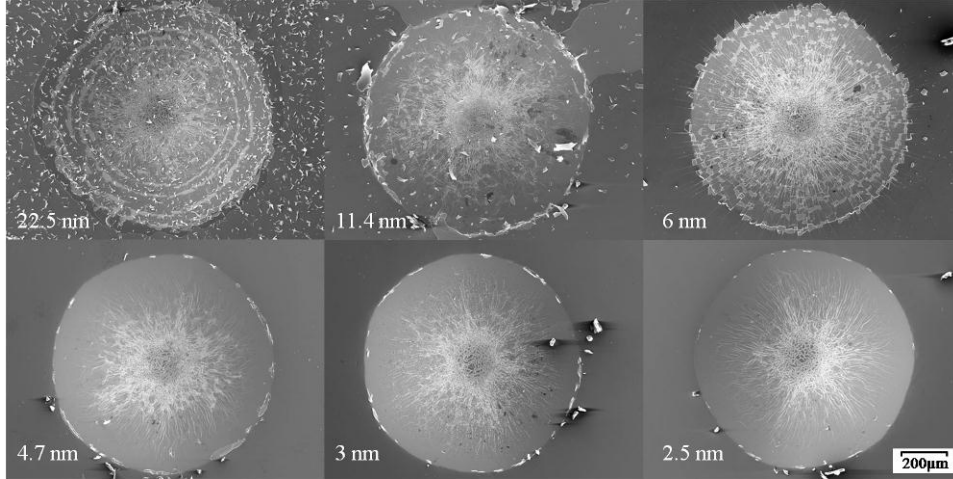
Figure 21 SEM micrographs of the indent morphologies after Rockwell C-Brale indentation of CrN/AlN superlattice coatings of different bilayer periods

Figure 22 represents the average COF values and the wear rates of CrN/AlN coatings. The low COF values of about 0.32-0.37 and wear rates in the low 10^{-7} mm^{3}N^{-1}m^{-1} range were obtained in the coatings with bilayer periods of 3-4.7 nm sliding against a WC-Co ball. The CrN/AlN coatings exhibit higher COF values varied from 0.41 to 0.58 and significantly increased wear rates in the 10^{-6} mm^{3}N^{-1}m^{-1} range as the bilayer period was increased from 6 to 22.5 nm.
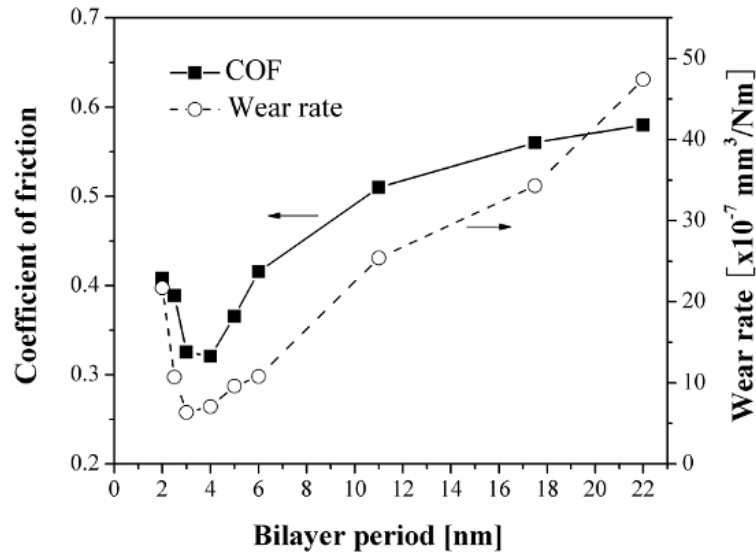
Figure 22 Coefficient of friction and wear rates of CrN/AlN coatings as a function of the bilayer period

3.2.3 Summary (II)

In summary, for the CrN/AlN superlattice coatings, the CrN layers epitaxially stabilize the AlN layers to NaCl-type structure as the thickness of the AlN layer and the bilayer period are

less than 3.3 and 4.7 nm respectively. The AlN layers transferred to a Wurtzite-type structure as the bilayer periods are larger than 6 nm. It was found that CrN/AlN coatings containing Wurtzite type AlN layers ($\Lambda>6$ nm) exhibit low hardness (23-25 GPa), poor adhesion and low wear resistance. On the other hand, NaCl-type CrN/AlN coatings exhibit super hardness above 40 GPa, good adhesion, low COF (0.32) and excellent wear resistance in a bilayer period range of 3~4.7 nm. The study demonstrated that it is important to control the AlN layer thickness below certain critical value (e.g. 3.3 nm in the present study) in CrN/AlN coatings to avoid the formation of Wurtzite type AlN structure, which was found to be detrimental to the structure and properties of CrN/AlN coatings.

3.3 Comparison of the CrAlN, Graded CrAlN and Superlattice CrN/AlN Coatings

3.3.1 Microstructure of the Coatings

TEM micrographs of the cross-section of an homogeneous $Cr_{0.42}Al_{0.58}N$ coating and a CrN/AlN superlattice coating with bilayer thickness of 7.8 nm are presented in **Figure 23**. It was found that all investigated coatings were characterized by a fully dense and highly non-defective microstructure. The homogeneous $Cr_{0.42}Al_{0.58}N$ coating exhibits a typical columnar structure with the columnar gain size of about 40~50 nm (**Figure 23a**). It was also found that the Al rich graded CrAlN coating exhibited a columnar feature, in which a denser and finer grain structure was observed compared to the homogeneous $Cr_{0.42}Al_{0.58}N$ coating (based on FESEM studies, not shown here).

On the other hand, a fully dense and columnar-free structure was observed in the CrN/AlN superlattice coating. The bright-field cross-sectional TEM micrograph of an example CrN/AlN coating is shown in **Figure 23b**. The CrN and AlN layers alternating in growth direction are shown as bright and dark layers in the micrograph, respectively. The AlN layers appear to be slightly lighter than the CrN layers because of the lower scattering factor of Al compared to Cr. It can be seen that the interface between CrN and AlN layers are well-defined and the bilayer thickness in this coating is about 7~8 nm. The insert SAED pattern displays a typical pattern of a nano poly-crystalline material consisting of the FCC Cr-Al-N phase. The more continuous rings in **Figure 23b** indicate that the multilayer CrN/AlN coating contains smaller grains than the homogeneous $Cr_{0.42}Al_{0.58}N$ coating and the grain size is in the nano-scale range.
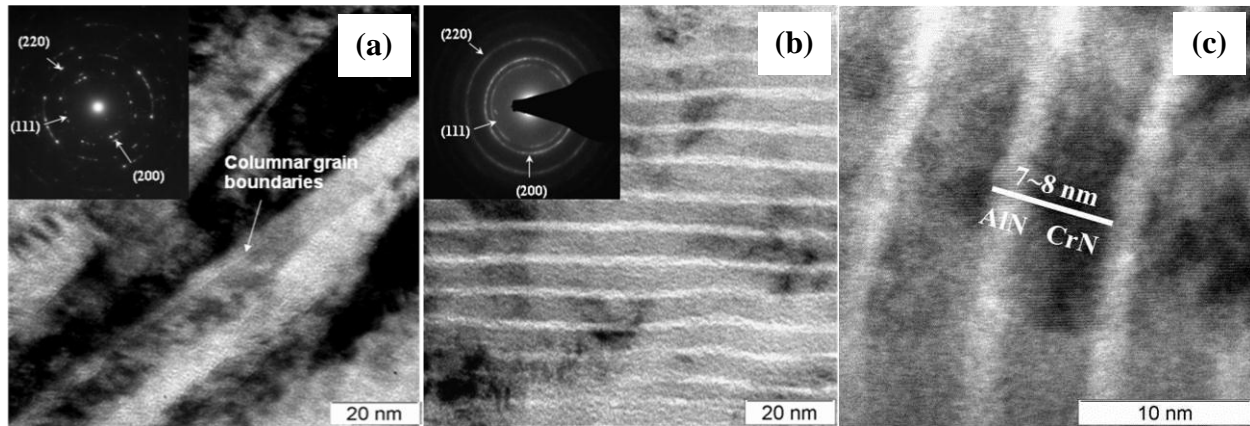
Figure 23 (a) TEM micrograph of the cross-section of a homogeneous Cr$_{0.42}$Al$_{0.58}$N Coating (b) TEM micrograph of the cross-section of a superlattice CrN/AlN coating with a bilayer period of about 7~8 nm, and (c) HRTEM micrograph of the CrN/AlN coating showing the well-defined interface (the bright layer is the AlN and the dark layer is the CrN

3.3.2 Mechanical and tribological properties of the coatings

Table 4 lists a summary of all of the measured coating properties, which are discussed below in more detail. A super hardness of 41.3 GPa was observed in the multilayer CrN/AlN coating with a bilayer thickness of 3.8 nm, which is much higher when compared to the single layer/homogeneous Cr$_{0.42}$Al$_{0.58}$N and the graded CrAlN coatings. Considering the super hardness enhancement, the bilayer thickness usually needs to be thin enough so that the dislocation generation can-not occur within the layers. In the study, the hardness of CrN/AlN superlattice coatings increased from 27 to 41.3 GPa as the bilayer thickness decreases from 7.8 to 3.8 nm. It is expected that the hardness of the coating can be further enhanced with a further decrease in the bilayer period to an optimum value.

Table 4 Summary of Properties of Homogeneous, Graded, and Superlattice CrAlN Coating

Properties	Homogeneous (58.5 at.% Al)	Al rich graded	CrN/AlN superlattice
Hardness (H) [GPa]	36.38±3.98	34.61±3.22	41.3±2.89 (Λ=**3.8 nm**)
Young's Modulus (E) [GPa]	369.9±29.3	378.47±24.72	377.653±14.21(Λ=**3.8 nm**)
H/E	0.0984	0.091	1.01 (Λ=**3.8 nm**)
Residual Stress [GPa]	-4.8	-2.25	Under characterization
Plasticity	50%	60%	63% (Λ=**3.8 nm**)
Rockwell C toughness	HF2	No cracking	No cracking
Coefficient of Friction	0.38	0.45	0.35 (Λ=**5.4 nm**)
Wear Rate (W$_N$) [10^{-6}mm^{3}N^{-1}m^{-1}]	2.87	3.12	0.95 (Λ=**5.4 nm**)

Figure 24 shows the micrographs of the indents measured with a Rockwell-C indenter for three CrAlN coatings. The homogeneous $Cr_{0.42}Al_{0.58}N$ coating exhibits extensive slim cracks with low degree of delamination along the indent boundary (**Figure 24a**), which can be associated with a HF2 adhesion strength quality (represents good and sufficient adhesion) as standardized in the VDI guidelines 3198, (1991). In contrast, excellent coating adhesion and improved toughness were indentified in the graded and superlattice CrAlN coatings after the Rockwell-C indentation tests, as shown in **Figure 24b** and **24c**. These two coatings show no cracks and very little delamination along the indent boundary, indicating very high toughness and adhesion.
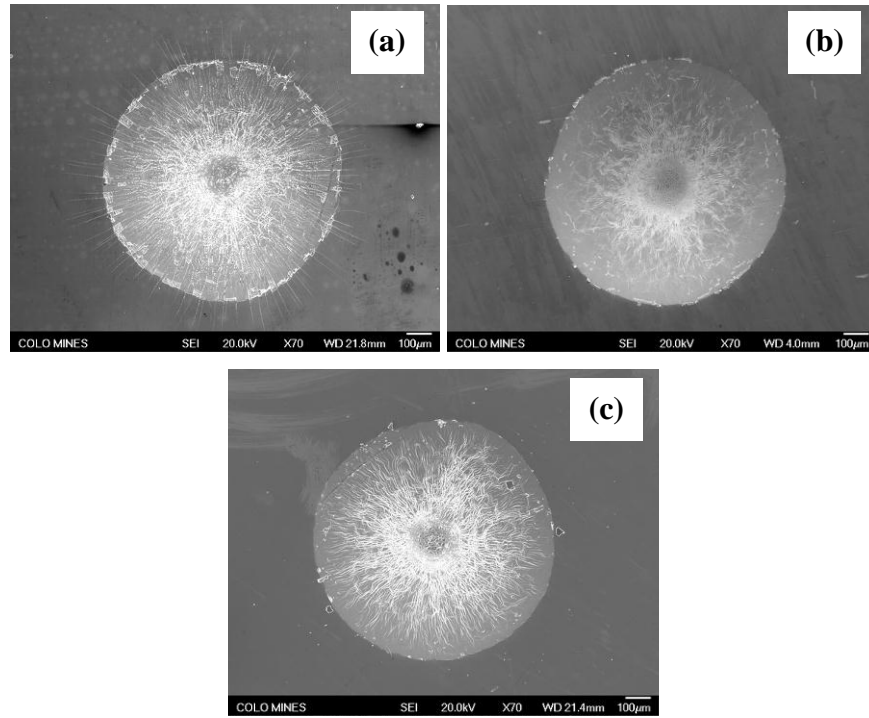
Figure 24 Micrographs of coating cracking and flaking from indentations with Rockwell C-Brale indenter: (a) cracking/flaking for a $Cr_{0.42}Al_{0.58}N$ coating; (b) no cracking damage and few delamination for a Al rich graded CrAlN coating; and (c) no cracking damage and delamination for a CrN/AlN superlattice coating (Λ=3.8 nm)

Figure 25 shows the COF of three coatings tested against a 1 mm WC-6%Co ball as a function of sliding period. The optical images of the wear tack morphologies were recorded after the tests and presented in the figure. The COF and wear rate values are listed in **Table 4** for comparison. All three coatings showed good wear resistance, e.g. the wear rate are all in the low 10^{-6} to 10^{-7} mm^3/Nm ranges. The homogeneous single layer $Cr_{0.42}Al_{0.58}N$ coating exhibits a low COF value of 0.38 and a low wear rate of $2.87x10^{-6}$ mm^3/Nm. When the coating was deposited

in an Al rich graded architecture, an increase in the COF value (0.45) and the wear rate (3.12×10^{-6} mm^3/Nm) were observed. The slight increase in the wear rate is possibly due to the decreased hardness in the film (with decreased Al concentration) when the wear depth was increased. In contrast, a low COF (0.35) and a wear rate (0.95×10^{-6} mm^3/Nm) were measured for a CrN/AlN superlattice coating with bilayer period of 5.4 nm. By examining the wear track morphologies (**Figure 25**) and profilometry scans, the cleaner wear track, with less wear debris along the track and lower wear depth in the CrN/AlN superlattice coating (Λ=5.4 nm) indicated an excellent wear resistance.
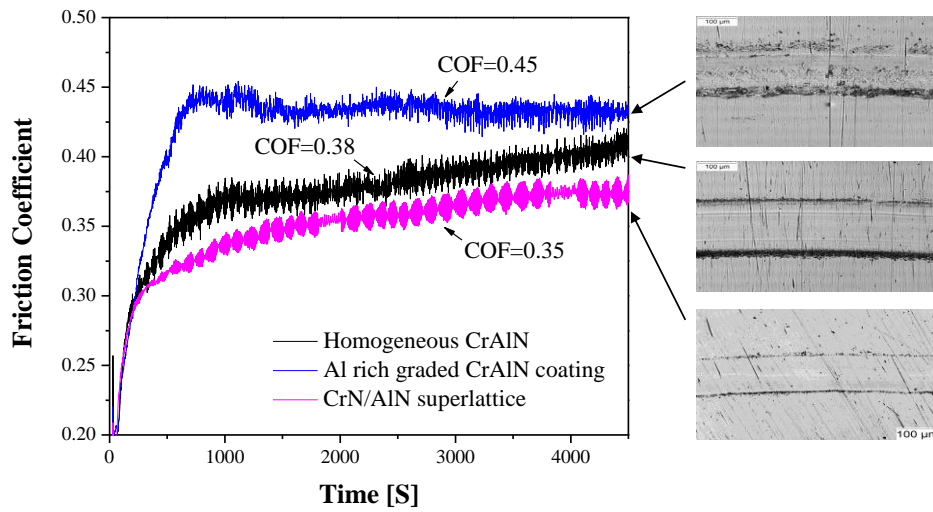
Figure 25 The sliding friction coefficient (COF) of three CrAlN coatings against with a WC-6%Co ball and corresponding wear track morphologies obtained after the wear tests

The improvement in the coating properties and adhesion can be attributed to the optimized coating structure in the graded and superlattice structured coatings. The TEM microstructure studies clearly demonstrate the formation of the CrN and AlN nanometer layers with a significant increase in the well-defined interfaces between layers (**Figure 23b**). The multiple interfaces in the coating can act as obstacles for the crack propagation. When cracks are initiated at the coating surface, they are propagating perpendicular to the substrate. In a single layer (homogeneous) CrAlN coating, the cracks will propagate all the way through the coating thickness easily. However, these cracks will change their propagation direction at layer interfaces if the coating is designed as a graded or multilayer structure. Therefore, the most important benefit of multilayer coating systems is that it can provide 'accommodation' of the thermal stresses that develops from thermal cycling, and can minimize the mismatch of CTE and stresses inherent in the deposition process.

41

3.3.3 Summary (III)

The microstructure, mechanical and tribological properties of the CrN/AlN superlattice coatings were investigated and compared with the homogeneous $Cr_{0.42}Al_{0.58}N$ single layer coating and an Al rich graded CrAlN coating. The superlattice approach produced a super hard (41 GPa), high toughness (no crack observed in the Rockwell- C indentation tests), and high wear resistance (low wear rate of 0.95×10^{-6} $mm^3N^{-1}m^{-1}$) with a bilayer period of 3.8 nm. The increased hardness, toughness, wear resistance and adhesion of two multilayered and graded coatings compared to a single layer CrAlN coating can be attributed to the multiple interfaces within the coating, which can hinder the dislocation movements and also deflect the crack propagation directions. Given the high oxidation resistance of CrAlN coating (>900 ^{o}C) and the superior properties demonstrated in the study, it is expect that the superlattice CrN/AlN and graded CrAlN coatings are very promising coating candidates for the aluminum high pressure die casting dies.

3.4 The Development of AlN Piezoelectric Thin Film Sensor Materials

3.4.1 Pulsing and Film Thickness Effect on Piezoelectric Response

The direct piezoelectric properties of the chosen samples have shown encouraging results. The following **tables 5-7** describe the direct piezoelectric coefficient obtained from the samples.

Table 5 Piezoelectric properties for different thickness, and effect of annealing

Architecture	Thickness	Processing parameter	Piezoelectric property (ε_{31} (C/m^2))
AlN/TiN/Ti/Si (TiN layer prevents Ti diffusion)	700 nm	-50V bias (introduces in-plane residual stress)/150W power)	-0.90
AlN/TiN/Ti/Si	500 nm	Same sample, after annealing	-0.87
AlN/TiN/Ti/Si	700nm	No substrate bias	Film shorted
AlN/Ti/Si	700nm	No substrate bias	-0.74
AlN/Ti/Si	470nm	No substrate bias	-0.14

Table 6 Frequency variation (pulsed power), no bias

Architecture	Processing parameter	Piezoelectric coeff. (C/m^2)
AlN/TiN/Ti/Si	100kHz/1microSec/1kW/closed field/3mT/N$_2$//0 bias/3hr	-0.69
AlN/TiN/Ti/Si	200kHz/1microSec/1kW/close field/3mT/N$_2$/0 bias/3hr	-0.82
AlN/TiN/Ti/Si	300 kHz/1microSec/1kW/close field/3mT/N$_2$/0 bias/3hr	-0.92

Table 7 Effect of bottom layer

Architecture	Thickness	Processing parameter	Piezoelectric coeff. (C/m^2)
AlN/TiN/Ti/Si	900nm	DC power: on TiN/Ti/Si substrate	-0.90
AlN/Ti/Si	700 nm	DC power: on Ti/Si substrate	-0.74
AlN/Pt/Ti/Si	Not measured	DC power: on Pt/Ti/Si substrate	-0.49

The piezoelectric co-efficient was an average of the values obtained by applying stress in two perpendicular in-plane directions. One can see that the Piezoelectric coefficient was the highest in film containing a TiN buffer layer and was irrespective of the heat treatment. The sample that was prepared without any substrate biasing did short circuit for some reason and the properties could not be measured. The films on pure Ti were electrically leakier, which could have been the reason for their underestimated value of the piezoelectric constant.

3.4.2 Working Pressure Effect

As mentioned in the previous section, to obtain the maximum piezoelectric effect in the coating sensor, the orientation of the AlN thin film must be controlled to produce (002) oriented thin film structures. Another factor that governs the thin film quality is the amount of intrinsic stress present within the film and its interface. A thin film with minimal amount of stress is desired to avoid any film delamination during operation. AlN thin films grown at different working pressures were deposited using the CFUBMS system, and their residual stress, crystal size and orientation/texture were examined using XRD and rocking curves. When varying the working pressure during the deposition we are not only altering the amount of reactive gas

present, we also alter the volatility conditions within the chamber. When the pressure is increased, it allows for more frequent ion bombardment on the substrate yet with less velocity. Too low a working pressure can lead to very slow deposition rates, introduction of high energetic ions approaching the substrate due to fewer collisions, and possibly not allow the plasma to ignite. The films were deposited varying the working pressure from 2 mTorr up to 6.5 mTtorr to investigate the effect of working pressure on residual stress, crystal size and orientation of the AlN thin films, as depicted in **Figure 26** (a-c).
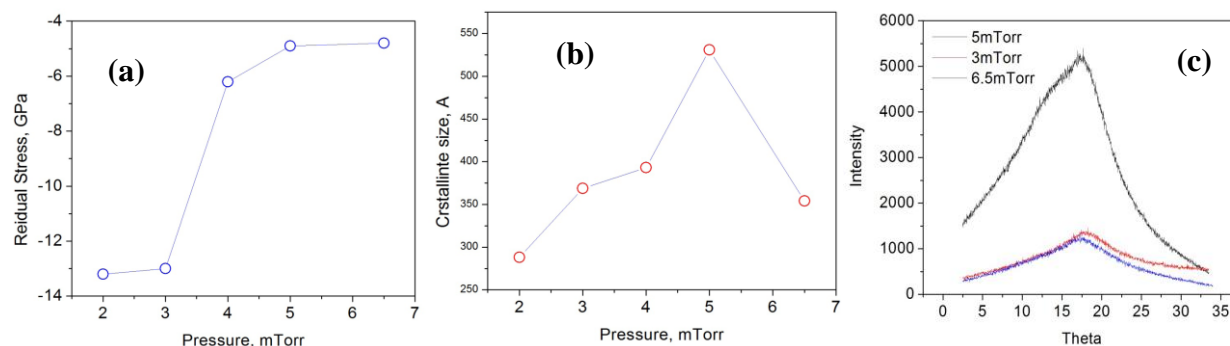
Figure 26 Relation between working pressure, (a) residual stress, (b) crystalline size and (c) rocking curves for different working pressure conditions

As the working pressure increases inside the chamber, more ion interactions occur and ions will lose their energy upon collision. At higher working pressures, the amount of ion bombardment on the substrate decreases due to the arrival of low energy ions thus producing films with lower a compressive stress level. On the other hand, at lower working pressures, the collision frequency of ions is much lower, and ions with high energy will impact the substrate introducing more defects and a higher compressive stress level. The size (columnar diameter) of the growing film increases with increasing pressure and reaches a maximum at 5 mTorr, as depicted in **Figure 26b**, and decreases at 6.5 mTorr. The maximum crystallite size at 5mTorr is consistent with our previous results where the films deposited at 5mTorr exhibit approximately 99% (002) orientation. Higher textured (002) growth produces larger crystallite size. The film deposited at 5mtorr also demonstrates a lower residual stress, as shown in **Figure 26a and 26c**. The narrower and more intense rocking curve, indicates the presence of lower residual stress and stronger (002) orientation. Thus, the film at 5 mTorr working pressure shows the lowest residual stress, larger crystal size and higher texturing in proffered (002) orientation.

3.4. 3 Thermal Stability of the AlN Films

In order to test the stability of AlN thin films at higher temperature, a DSC method was

used to investigate thermal stability, as shown in **Figure 27a**, and the films were analyzed by XRD to evaluate any phase change, as depicted in **Figure 27b**.
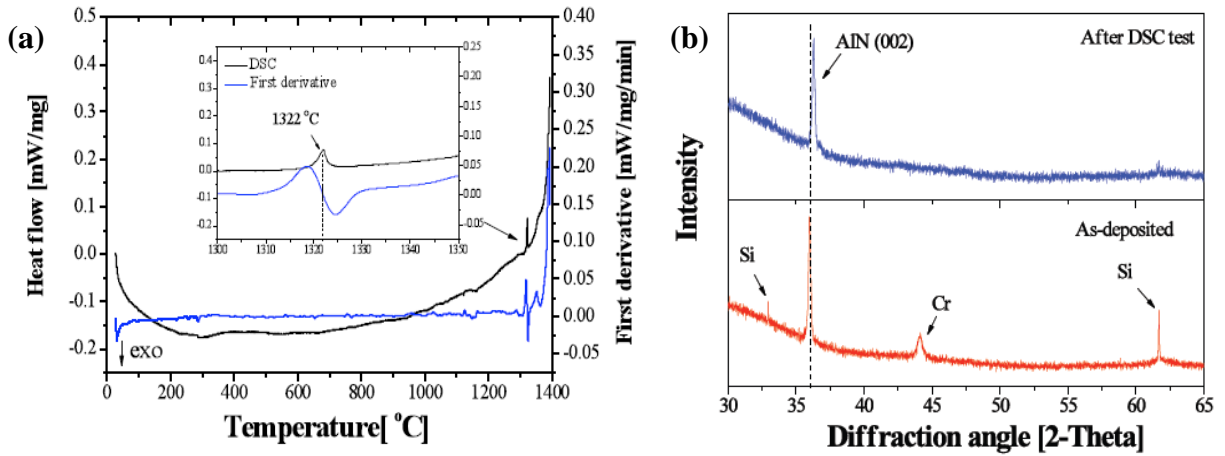
Figure 27 (a) DSC curve and first derivative obtained at 20 K/min heating rate in the flowing argon (55 sccm) and (b) its corresponding XRD graph before and after DSC analysis

An AlN thin film with a Cr electrode deposited on silicon substrate was heated from room temperature up to 1400°C with a heating rate of 20 K/min in a flowing argon (55 sccm) environment. The DSC curve indicates that there was no apparent phase change below 1322 °C, confirming the superior thermal stability of these AlN films. An endothermic peak at 1322 °C suggests the formation of Cr-Si compound since this temperature is very close to Si melting temperature. A comparison of XRD graphs of as-deposited film with the same film after DSC annealing at 1400°C, will identify any crystal phase change during DSC analysis. The silicon and Cr peaks disappeared after the DSC test, as shown in **Figure 27b**, indicating the partial melting of silicon substrate and thus the formation of Cr-Si compound. However, one can see that the peak for AlN (002) orientation is not altered after DSC test compare to as-deposited film, which indicates the excellent structural stability of AlN films upon heating.

3.4.4 Substrate Biasing Effect

Three AlN thin films with different substrate biasing (Floating, -50 V and grounded), were deposited on silicon with other similar sputtering conditions. We have studied the effect of substrate biasing on (002) crystal orientation of piezoelectric AlN films. As we can see in the **Figure 28**, the film that was grounded shows the highest relative intensity compared to the other two films. The film that was deposited at floating bias showed some (002) orientation but less than grounded substrate. One of the reasons that this phenomena happened is the nature of (002) oriented AlN films that are thermodynamically the most stable phase. However, as we apply

some voltage to the substrate we deviate from this thermodynamic equilibrium and the amount of preferred (002) orientation drops as the substrate biasing voltage increases.
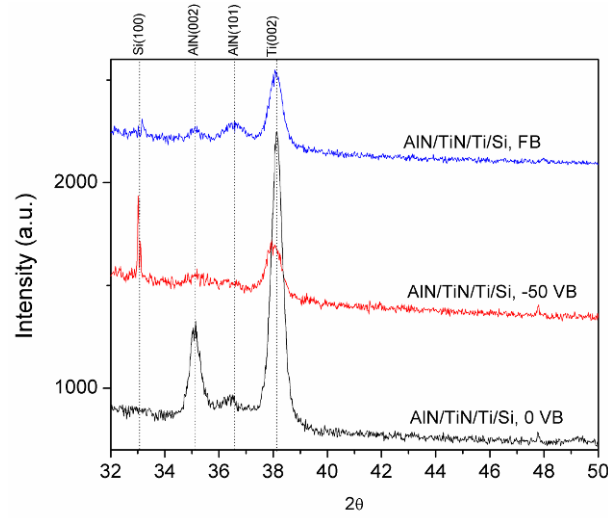
Figure 28 Substrate bias voltage effect on preferred (002) orientation of AlN thin films

3.4.5 Seed-layer Effect on the (002) Orientation of AlN Films

Three AlN films with different seed layers materials Cr, Al and Ti/TiN were deposited on stainless steel substrates. The films that were deposited on top of Cr and Al seed layers, as depicted in **Figure 29**, did not show any (002) orientation. But the films that have been deposited using Ti/TiN seed layer showed some (002) orientation and maybe some AlN (101) or TiN crystal formation since these two peaks are very close to each other and hard to resolve.

This indicates that Ti (002) orientation having same HCP close packed structure compared to (002) AlN structure can promote epitaxial growth.
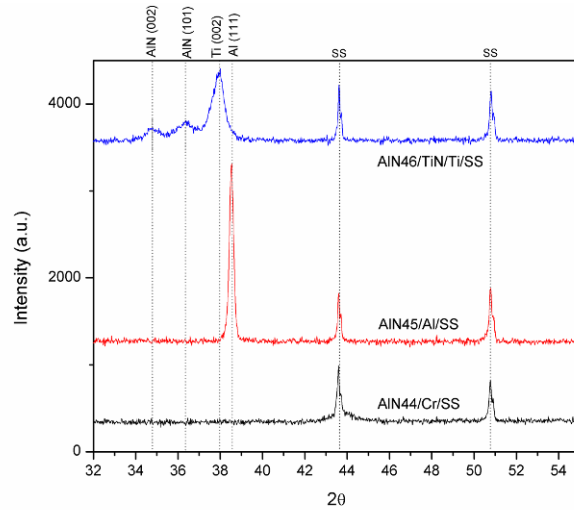
Figure 29 Seed layer (Al, Cr and Ti/TiN) effect on preferred (002) orientation of AlN thin films

46

Moreover, four AlN films with additional seed layer materials- Pt and Mo - were deposited on the stainless steel substrates. The first pair of films was deposited at two different working pressures of 3 and 5 mTorr to study the effect of deposition pressure on the orientation of these films. As one can see from the **Figure 30**, the film that was deposited at 5 mTorr showed higher degree of preferred (002) orientation.
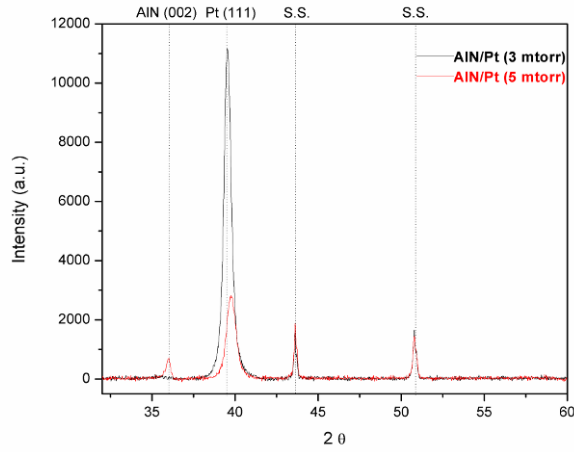
Figure 30 Working pressure effect on the (002) orientation of AlN thin films
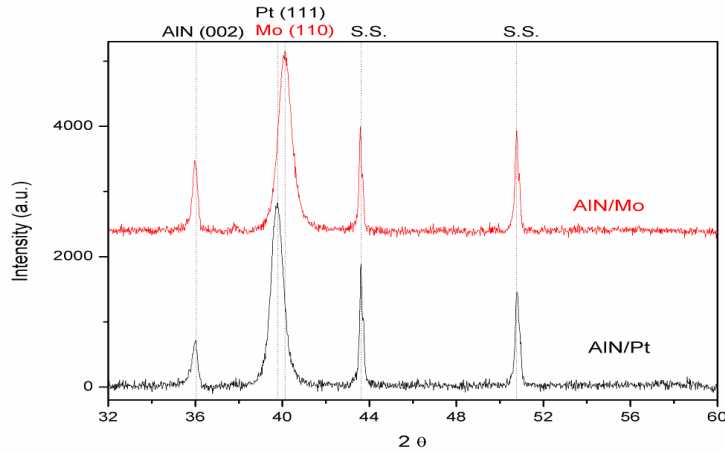
Figure 31 Deposition temperature effect on preferred (002) orientation of AlN thin films

The best films of each group were compared to see the effect of seed layer on the (002) texture of AlN thin films. As we can observe from **Figure 31**, both films deposited on Pt and Mo showed AlN (002) peaks on the stainless steel substrate but the AlN film that was deposited on Mo seed layer illustrated a bit higher preferential orientation, because the (110) planes in body centered cubic molybdenum is a closed pack plane and has a good lattice matching with AlN (002) planes and hence more epitaxial film could be grown using this under-layer.

3.4.6 Cross-sectional TEM

Figure 32 shows the cross sectional view of AlN thin film exhibiting columnar grains with the average size about 40-60 nm. High resolution image of this film shows the lattice fringes corresponding to (002) AlN planes with d-spacing of about 0.249 nm.
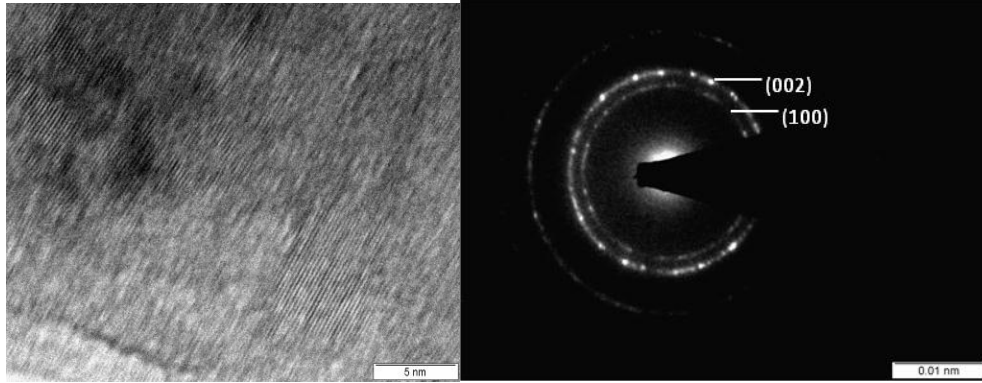
Figure 32 Cross-sectional TEM image and SAED of AlN films deposited at 5 mTorr

The diffraction pattern also showed polycrystalline feature of this AlN thin film with mostly (002) planes presented there and with the small amount of (100) planes also presented in the electron diffraction patterns which are not evident in the XRD studies.

3.4. 8 Remote Piezoelectric Measurements (Michelson Interferometer)

By applying a voltage difference across the top and bottom electrodes in the AlN thin film system, one can measure the displacement change remotely due to the inverse piezoelectric effect by using the Michelson Interferometer setup. One of these interferometer measurements raw graph data at 1900 and 2000 kHz input frequency is depicted in **Figure 33**. From the peak intensity we can measure the piezoelectric coefficients in the unit of pm/v. In order to calibrate the interferometer, a panametric transducer was tested with commercial laser vibrometer to measure its vibration speed and hence measure the dimensional change in the home made interferometer. Then, piezoelectric coefficient d_{33} (pm/v) was calculated based on the reference transducer measurements. These results for various driving frequency is shown in **Figure 34**, the AlN coating has shown good piezoelectric response over wide frequency range.

10 VPP sinusoidal drive
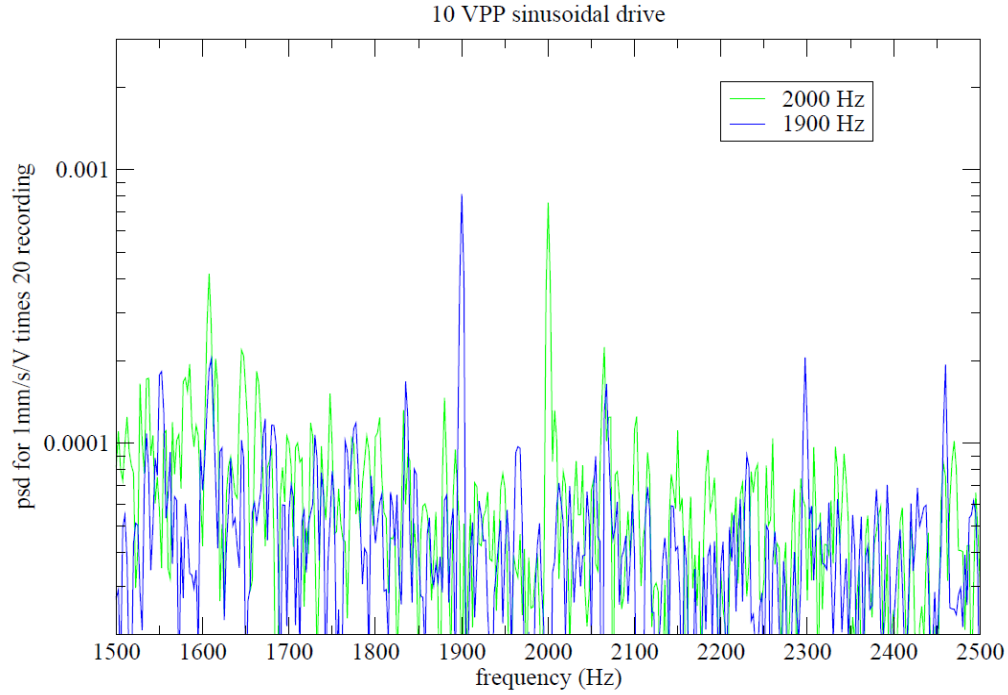
Figure 33 Fourier transform interferometery graph of AlN film with the application of 10 V sinusoidal waves
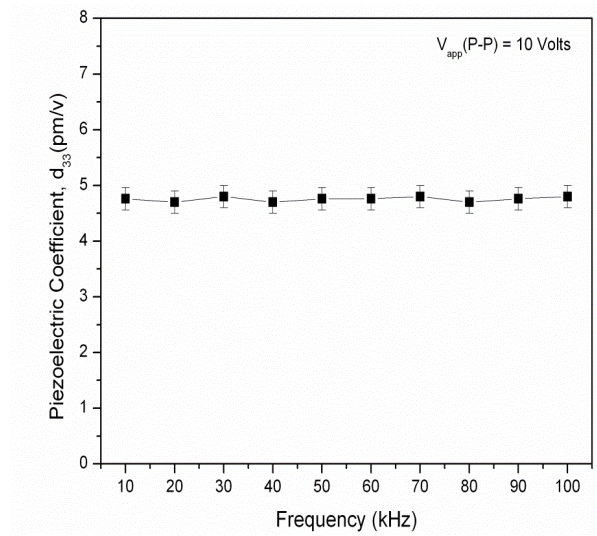
Figure 34 Piezoelectric coefficient d_{33} measurements vs. different driving frequency at 10 volts applied voltage

3.4.9 Summary (IV)

AlN thin films exhibiting strong preferred (002) orientation and excellent thermal stability was identified as one of the 'smart' layer candidates and has been synthesized using pulsed CFUBMS. The working pressure, seed layer, and the pulsing frequency exhibited significant influence on the piezoelectric response and the degree of (002) orientation of the AlN

thin film. It was found that the films deposited on TiN/Ti and Pt layers showed strong (002) orientation and high piezoelectric response. Michelson Interferometer measurement has been developed to be used as an effect method to remotely measure the piezoelectric response of the AlN thin films in the laboratory scale.

4. Benefits Assessment

4.1 Energy Saving

The technology offers energy savings through reduced energy use in the die casting process from several factors such as greatly increased life of the tools and dies, reuse of the dies and die components, reduction or elimination of lubricants, and reduced machine down time. Use of the optimized coating system will also result in the reduction of Al solder sticking on the die and die component surface and therefore reduce the energy involved in the cleaning process of the dies. The combination of the depositions of the CrN/AlN superlattice coating and the AlN piezoelectric thin film using one deposition technique in one deposition system also reduced energy use in the processing equipment. This task was predicted to result in an average energy savings of 1.3 trillion BTU's/year over a 10 year period after initial commercial transition. Current (2012) annual energy saving estimates, based on initial dissemination to the casting industry in 2010 and market penetration of 80% by 2020, is 3.1 trillion BTU's/year (Appendix 1).

4.2 Potential Cost Savings

The greatest cost to the die caster is the replacement of the dies, estimated at $20,000-$200,000 for each new die. Use of the optimized coating system will result in more than a 30% reduction in capital cost of the dies, which is the extension of the life of a coated die as compared to that of an uncoated die. This estimate is based on a previous NADCA DOE project (DOE DE FC07 OOID13850) that studied coated and uncoated die core pins from in-plant trials. The use of the 'smart' coating sensor will significantly reduce the possibility of the complete failure of the die and die components. Additional savings in costs also result from reducing the potential use of die lubricants and additional cleaning process for the soldering problems.

4.3 Environmental Benefits

With the use of the optimized die coating system, environmental threats and associated cost for disposal of various die lubricant wastes will be significantly reduced. In addition, the environmental waste incurred every time the die material prematurely fails could also be reduced by using the 'smart' coatings. The reduction of scrap and improvement in die life will also result in a reduction of environmental emissions associated with the melting and pouring of the aluminum. The average annual estimate of CO_2 reduction per year through 2020 is 0.63 Million Metric Tons of Carbon Equivalent (MM TCE) based on the energy savings above.

5. Commercialization
5.1 Commercialization plan

The project commercialization plan is to utilize a commercial scale production unit that will be used for application of the optimized coating system for dies and die components. The coating cost per tool depends upon the number of tools that can be accommodated in a single deposition run. The currently available coating deposition system at CSM has limited coating zone 30 inch (dia.) x 24 inch height that limits the number of parts that can be accommodated in a single deposition run. A larger deposition chamber can accommodate more parts and therefore the coating cost per part can be further reduced.

In this program a contact was made with Phygen Coating LLC, which is a Minneapolis-based provider of high-end wear-resistant coatings to a wide range of industrial customers. The initial commercialization step is: Phygen will try to reproduce the optimized coating deposition conditions and parameters on steel coupons in their industrial scale coaters. When comparable properties and performance of the CrN/AlN superlattice coating have been achieved, real die components, e.g. die core pins will be coated in the industry coaters. In the final step, these coated die core pins will be sent to another industry contact, Airo Die Casting for the in-plant trials.

5.2 Commercialization status

After nearly a twelve month effort, Phygen successfully reproduced CrN/AlN superlattice coatings in their industrial sized coaters, which exhibited similar optimized structure and properties to the coatings deposited in the CSM . **Figure 35** shows the examples of die core pins coated with the CrN/AlN superlattice smart coatings. The coated core pins were delivered to Airo Die Casting for evaluation.

The coated core pins have been under taken about 10000 die casting shots after 6 month of in-plant trial in Airo Die Casting. **Figure 36** shows the coated core pins used in the die casting in-plant trial and the core pin after about 10000 shots. According to the performance feedback from Airo Die Casting, the initial test data was very encouraging. Airo Die Casting suggested that soldering of the ejector core pins is more severe over areas opposite the in-gate/opposite the flat on the core pin. The core pins performed well with a die casting shot up to 10000. Usually, the un-coated H13 core pins exhibited sign of failure after 3000 shots. Therefore, the results indicate that an at least more than 30% increase in the die life time could be achieved. It should

be mentioned that the enhanced tool life due to the developed coatings would also minimize the downtime of the machining operation and therefore provide more savings. Savings related to the less down time was not considered.

Figure 35 Example of die core pins coated with CrN/AlN based smart coatings
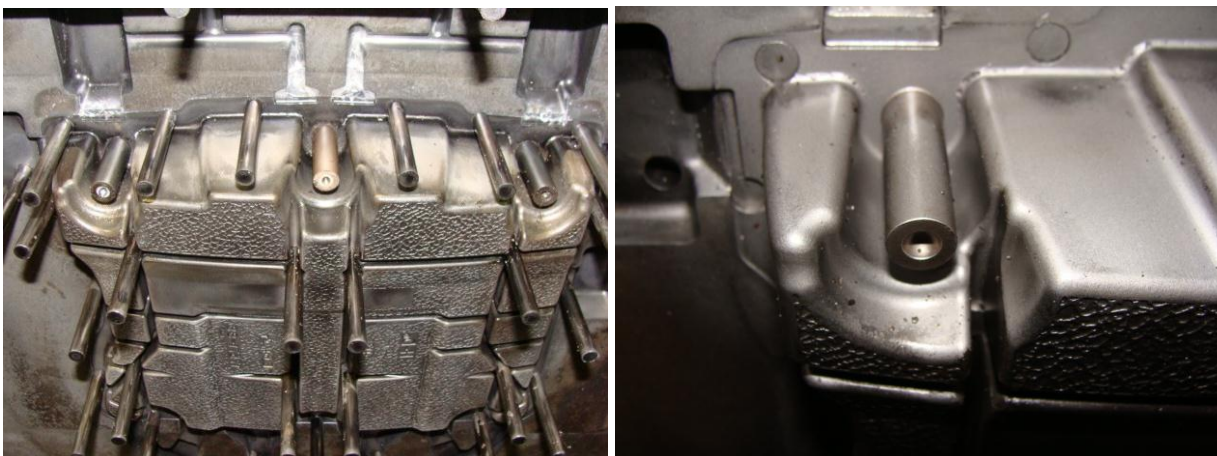
Figure 36 (a) Photo showing the coated core pins used in the die casting in-plant trial, (b) a photo shows the core pin after about 10000 shots

5.3 Barriers and potential approaches

There are two major challenges for the project. The first one is to significantly reduce the production cost of the 'smart' coating system, since the entire process contains multiple steps. By having a deposition chamber that can accommodate more parts in a single deposition run, the coating cost can be lowered. The second challenge is to obtain in-situ piezoelectric signal using remote control during the real die casting process.

For further reduction of the coating cost in the future, one approach is to increase the throughput of the deposition system, which includes the design and fabrication of specific fixtures to hold large number of die components in one deposition run. Another approach is to

use larger deposition chamber which can accommodate more parts and therefore the coating cost per part can be reduced.

CSM is currently working with NADCA on a commercialization and in-plant validation in an effort to achieve full commercialization of the coating systems. Two commercial coating companies, Phygen and Swiss-Tek, are part of this transition project.

6. Accomplishments

6.1 Technical accomplishments

This task is the first to address the design methodology for effective coating for die casting dies (multilayer and smart coating concept). The project has successfully developed a multifunctional smart coating system containing a CrN/AlN superlattice based tribological layer and an AlN piezoelectric thin film sensor for die casting dies.

The commercialization efforts with Phygen LLC have led to the production of the CrN/AlN superlattice coatings in industrial coaters. The in-plant trial of the coated core pins also demonstrated significantly increased die life as compared to the bare H13 core pins.

Two Ph.D. students have been financially supported by the research project and graduated in the project period. One US patent has been applied for the design coating system (*J. J Moore, D. Zhong, J. Lin, 'Functionally Graded Alumina-based Thin Film System', Pub. No. : US2005/0263261 A1*).

More than 30 research papers have been published in peer reviewed journals and more than 10 presentations have been given in international conferences to publicize the major outcomes of the research. Below is a list of the international publications for the research supported by the project.

6.2 Published International SCI Journals:

1. Jianliang Lin, William D Sproul, Peter Ried, Steve Udvardy, John J Moore, "Modulated pulsed power magnetron sputtering for the die surface engineering applications", *Die Casting Engineering*, March Issue (Invited contribution), (2012). pp 44-48.
2. J. Lin, N. Zhang, W.D. Sproul, and J.J. Moore, "A comparison of the oxidation behavior of CrN films deposited using continuous dc, pulsed dc and modulated pulsed power magnetron sputtering", *Surf. Coat. Technol*.206 (2012) 3283-3290.
3. J. Lin, W.D. Sproul, J.J. Moore, "Tribological behavior of thick CrN coatings deposited by modulated pulsed power magnetron sputtering", *Surf. Coat. Technol*. 206 (2012) 2474-2483.
4. J. Lin, Ningyi Zhang, Zhili Wu, W.D. Sproul, Michael Kaufman, Mingkai Lei, J.J. Moore, "Thick CrN/AlN superlattice coatings deposited by the hybird modulated pulsed power and pulsed dc magnetron sputtering",*Surf. Coat. Technol*.
5. J. Lin, M. Pinkas, and J.J. Moore, "The phase and microstructure of CrAlN films deposited by pulsed dc magnetron sputtering with synchronous and asynchronous bipolar pulses", *Thin Solid Films* 520 (2011) 166-173.
6. J. Lin, J.J. Moore, and W.D. Sproul, "Structurally laminated CrN films deposited by multi pulse modulated pulsed power magnetron sputtering",*Surf. Coat. Technol*. 206 (2011) 1780-1786.
7. J. Lin, J.J. Moore, J. Wang, W.D. Sproul, "High temperature oxidation behavior of CrN/AlN superlattice coatings", *Thin Solid Films*, 519 (2011) 2402-2408.
8. J. Lin, J. J. Moore, M. Pinkas, D. Zhong and W. D. Sproul, "TiBCN:CNx multilayer coatings deposited by pulsed closed field unbalanced magnetron sputtering", *Surf. Coat. Technol*. 206 (2011) 617-622.

9. J. Lin, B. Mishra, J.J. Moore, W.D. Sproul, and J.A. Rees "The Effect of Magnetron Pulsing on the Structure and Properties of Tribological Cr-Al-N Coatings", *J. Nanoscience and Nanotechnology* 10 (2) (2010) 1278-1285.

10. J. Lin, J. J Moore, B. Mishra, M. Pinkas, W. D Sproul, "Structure, Mechanical and Tribological Properties of TiBCN Nanocomposite Coatings", *Acta Mater*. 58 (2010) 1554-1564.

11. J. Lin, J.J. Moore, B. Mishra, M. Pinkas, W.D. Sproul, "Nano-structured CrN/AlN multilayer coatings synthesized by pulsed closed field unbalanced magnetron sputtering", *Surf. Coat. Technol*. 204 (2009) 936-940.

12. J.Lin, J.J. Moore, W.C. Moerbe, M. Pinkas, B. Mishra, G.L. Doll, W.D. Sproul, "Structure and properties of selected (Cr-Al-N, TiC-C, Cr-B-N) nanostructured tribological coatings", *Int. J. of Refract. Met.* 28(1) (2009) 2-14.

13. J. Lin, B. Mishra, S. Myers, J.J. Moore and P. Ried, "The Development of a Nanostructured, Graded Multilayer $Cr-Cr_xN_y-Cr_{1-x}Al_xN$ Coating Produced by Pulsed Closed Field Unbalanced Magnetron Sputtering (P-CFUBMS) for Use in Aluminum Pressure Die Casting Dies", *J. Nanoscience and Nanotechnology*, 9 (2009), 3514–3523.

14. J. Lin, B. Mishra, J.J. Moore, X.H. Zhang, W.D. Sproul, 'CrN/AlN superlattice coatings synthesized by pulsed closed field unbalanced magnetron sputtering with different CrN layer thicknesses', *Thin Solid Films*, 517 (2009) 5798-5804.

15. J. Lin, Z.L. Wu, X.H. Zhang, B. Mishra, J. J Moore, W. D. Sproul, 'A Comparitive Study of CrN_x coatings Synthesized by DC and Pulsed Magnetron Sputtering', *Thin Solid Films*, 517 (2009), 1887-1894.

16. J. Lin, B. Mishra, J.J. Moore, and W.D. Sproul, "A study of the oxidation behavior of CrN and CrAlN thin films in air using DSC and TGA analyses", *Surf. Coat. Technol*. 202 (2008) 3272.

17. J. Lin, J. J Moore, B. Mishra, M. Pinks, W. D. Sproul, and J.A. Rees, "Effect of Asynchronous Pulsing Parameters on the Structure and Properties of CrAlN Films Deposited by Pulsed Closed Field Unbalanced Magnetron Sputtering (P-CFUBMS)", *Surf. Coat. Technol*.202 (2008): 1418-1436.

18. J. Lin, B. Mishra, J.J. Moore, W.D. Sproul, and J.A. Rees, "Effects of substrate to chamber wall distance on structure and properties of CrAlN coatings deposited by pulsed -closed field unbalanced magnetron sputtering (P-CFUBMS)", *Surf. Coat. Technol*. 201 (2007): 6960-6969.

19. J. Lin, B. Mishra, J.J. Moore, W.D. Sproul, and J.A. Rees, "Examination of the pulsing phenomena in pulsed-closed field unbalanced magnetron sputtering (P-CFUBMS) of Cr–Al–N thin films", *Surf. Coat. Technol.* 201 (2007) 4640-4652.

20. J. Lin, B. Mishra, J.J. Moore, and W.D. Sproul, "Microstructure, mechanical and tribological properties of $Cr_{1-x}Al_xN$ films deposited by pulsed-closed field unbalanced magnetron sputtering (P-CFUBMS)", *Surf. Coat. Technol*. 201 (2006) 4329-4334.

21. J. Lin, A.O. Kunrath, D. Zhong, S. Myers, B. Mishra, and J.J. Moore, "Development of Multi-layered and Graded Die Coatings for Materials Processing Applications", *Advances in Science and Technology*, vol. 45 (2006) pp. 1145-1154

22. J. Lin, S. Carrera, A.O. Kunrath, D. Zhong, S. Myers, B. Mishra, P. Ried, and J.J. Moore, "Design methodology for optimized die coatings: The case for aluminum pressure die-casting, *(Invited paper B7-1-1, ICMCTF, presented Monday May 2nd, 2005, San Diego), Surf. Coat. Technol.* 201 (2006): 2930–2941.

6.3 Published in Die Casting Conference Proceedings:

1. J. Lin, W.D. Sproul, P. Ried, S. Udvardy, "Superhard, wear resistant and thermally stable CrN/AlN superlattice coatings deposited using the MPPMS technique", *116th Metalcasting Congress*, Oct (2012).

2. M.Hasheminiasari, J. Lin, and J. J. Moore, "The influence of deposition parameters on the texture of a sputtered, 'smart' AlN thin film to be used in die coatings for Al pressure die casting", *115th Metalcasting Congress*, Oct (2011)

3. M. Hasheminiasari, J.Lin, J.J. Moore and P. Ried, "Development of Nanostructured Die Coating

System for Al Pressure Die Casting: Towards a 'Smart' Die Coating", *114th Metalcasting Congress*, Orlando, FL, USA, March (2010)

4. J. Lin, F. Wang, S. Bhattacharyya, M. Hasheminiasari, S. Myers, B. Mishra, J.J. Moore, "Development of a 'Smart' Die Coating for Al Pressure Die Casting", *113th Metalcasting Congress*, NADCA, Las Vegas, Nevada, April 7-10, (2009).

5. J. Lin, F. Wang, S. Myers, B. Mishra, J.J. Moore, and P. Ried, 'A Examination of Coating Architecture in the Development of An Optimized Die Coating System for Aluminum Die Casting", *112th Metalcasting Congress*, NADCA, Atlanta, Georgia, May 17-20, (2008).

6. Best Congress Paper Award: J. Lin, S. Myers, S. Bahattacharyya, B. Mishra, J.J. Moore and P.Ried, "Optimization of a graded, multilayer die coating system for use in Al pressure die casting", *111th Metalcasting Congress*, NADCA, Houston, Texas, May 15-18, (2007).

7. J. Lin, B. Mishra, S. Myers, S. Bhattacharyya, J.J. Moore and P. Ried, "Developemnt of Thin Film Coatings for Dies Used in Aluminum Pressure Die-Casting of Automotive Components", *Material Science & Technology 2007 Conference and Exhibition*, (2007).

8. J. Lin, S. Myers, B. Mishra, J.J.Moore, "Design of Optimized Die Coatings Used in Material Forming Processes", *The Flexible Automation and Intelligent Manufacturing (FAIM) International Conference (2006)*, June 26-28, 2006, University of Limerick, Limerick, Ireland

9. J. Lin, A.O. Kunrath, D. Zhong, S. Myers, B. Mishra, and J.J. Moore, "Development of Multi-layered and Graded Die Coatings for Materials Processing Applications", *11th International Conference on Modern Materials and Technologies*, Acireale, Italy, (June 04-09, 2006).

10. J. Lin, S. Bhattacharyya, S. Myers, B.Mishra, and J.J. Moore, "The development of surface engineered coating systems for aluminum pressure die casting dies: optimization of the Cr-Al-N intermediate layer towards a 'smart' die coating", *110th Metalcasting Congress*, NADCA, Columbus, OH, April 18-21, (2006).

11. J. Lin, S. Myers, and J.J. Moore, "Surface treatments and coating technology used in die casting", *110th Metalcasting Congress*, NADCA, Columbus, OH. (2006).

12. J. Lin, S. Carrera, A.O. Kunrath, D. Zhong, S. Myers, B. Mishra, P. Ried, and J.J. Moore, "Design Methodology for Optimized Die Coating Used in Aluminum Pressure Die Casting", *Transactions of the North American Die Casting Association (NADCA) Congress and Exposition*, 2005.

13. J.L. Lin, S. Myers, O. Salas, S. Carrera, P. Ried, J. Brennan, B. Mishra, J.J. Moore, "Degradation Mechanisms of Die Coating Used in Aluminum Pressure Die Casting", *Surface Engineering in Materials Science III*, Edited by A. Agarwal, N.B. Dahotre, S. Seal, J.J. Moore, and C. Blue TMS (The Minerals, Metals & Materials Society), 2005.

7. Conclusions

The technical aspects of the project have been successfully completed. A 'Smart' coating design based on thin film piezoelectric sensor embedded within a tribological coating system has been introduced. The structure and properties of the coating system have been optimized using a CFUBMS deposition system to achieve the maximum performance in terms of superhardness (>40 GPa), excellent wear resistance, good toughness, excellent adhesion, and high thermal stability. The microstructure, mechanical and tribological properties of the CrN/AlN superlattice coatings were investigated and compared with the homogeneous CrAlN single layer coating and an Al rich graded CrAlN coating. The superlattice approach produced a super hard (41 GPa), high toughness, and high wear resistance with a bilayer period of 3.8 nm. The AlN piezoelectric thin film has been optimized to achieve good piezoelectric response by obtaining a highly (0002) texture in the film. AlN was selected as a sensor material due to its high thermal stability and good piezoelectric properties compared to other candidates. AlN thin films with strong (002) orientation were deposited. The effect of working pressure, pulsing frequency and seed layer materials on the preferred orientation and piezoelectric response of AlN films were investigated. Direct piezoelectric measurements were designed and tested for room temperature and a converse piezoelectric measurement, laser interferometry, will be used for high temperature measurements. There was a charge breakdown problem associated with the films at small thickness, which was minimized at thicknesses above about 900 nm.

In the project, commercialization efforts have been carried out with Phygen LLC for the production of the CrN/AlN superlattice coatings in industrial deposition equipments. Coatings have been applied to the real die core pins. The die casting performance of the developed coatings on the coated core pins were evaluated in actual commercial die casting runs and compared with that of uncoated core pins. Significant improvement in the die core pin life was demonstrated.

The barriers encountered during the operating period include further reducing the production cost of the 'smart' coating system and obtaining in-situ piezoelectric signal using remote control during the real die casting process. Although the DOE-funded effort is now completed, the CSM "Advanced Coatings and Surface Engineering Laboratory" (ACSEL) will continue to work the optimized smart die coating system, especially the AlN piezoelectric thin film remote measurement, and will continue to work closely with industry partners and the North

American Die Casting Association (NADCA) and ATI for different applications. In addition, the Defense Logistics Agency has funded CSM to develop further investigate lube-free die casting under the American Metalcasting Consortium's "Casting Solutions for Readiness" program.

Appendix 1: Assumptions for Calculating Energy Savings

- There was an estimated 1.6 million tons of die casting shipments in 2000 (U.S. Department of Commerce, U.S. Census Bureau, Current Industrial Reports, Iron and Steel Castings, MA331E (00)-1.)
- The die casting industry will grow at a rate of 2.5% per year (AFS Metalcasting Forecast & Trends 2002 (Oct. 2001))
- Baseline energy consumption for die casting is 23.4 million Btu per ton = 6858kWh
- The results of this project will provide the ability to design better dies which will in turn reduce scrap and improve operating efficiency in contributing to a combined 8% improvement in energy efficiency.
- Assumes 3412 Btu/kWh (Source: DOE/EIA, Monthly Energy Review)
- Approximately 25% of scrap and 75% new material are used during melting. The average price for Aluminum scrap in 2001 was .49 a pound or $980 a ton (Source: American Metal Market). For new aluminum it cost about .70 a pound or 1400 per ton. (Source: U.S. Geological Survey, Mineral Commodity Summaries, Jan 2002) A majority of die castings are aluminum therefore aluminum price data was used for these calculations
- Number of installed die casting units in US market: 1,600,000 in 2000
- Annual market growth rate: 2.5%
- Ultimate Potential Accessible Market: 100%
- Likely Technology Market Share: 80%
- Savings Attributed to Program: 100%

References

[1] J. Lin, , S. Carrera, A.O. Kunrath, D. Z hong, S. Myers, B. Mishra, P. Ried, and J.J. Moore, "Design Methodology for Optimized Die Coatings: The Case for Aluminum Pressure Die-Casting, (Invited paper B7-1-1, ICMCTF, presented Monday May 2nd, 2005, San Diego), Surface and Coatings Technology, vol 201 (2006) 2930–2941.

[2] P.H. Mayrhofer, C. Mitterer, L. Hultman,and H. Clemens "Microstructural design of hard coatings", Progress in Materials Science, vol 51, No. 8 (2006) 1032-1114.

[3] V.I. Gorokhovsky, D.G. Bhat, R. Shivpuri, K. Kulkarni, R. Bhattacharya, and A.K. Rai, "Characterization of large area filtered arc deposition technology: part II — coating properties and applications", Surf. Coat. Technol. vol 140 (2001) 215-224

[4] J. Lin, S. Myers, O. Salas, S. Carrera, P. Ried, J. Brennan, B. Mishra, J.J. Moore, "Degradation Mechanisms of Die Coatings Used in Aluminum Pressure Die Casting," TMS (The Minerals, Metals & Materials Society) congress, (2004).

[5] J. Lin, S. Carrera, O. Salas, B. Mishra, G. Mustoe, P. Ried, J. Brennan, and J.J. Moore, "The Development of Surface Engineered Coating Systems for Aluminum Pressure Die Casting Dies: An Evaluation of Six Commercial Coatings", Transactions of the North American Association (NADCA) Congress and Exposition, (2003).

[6] G.E. Dieter, Mechanical Metallurgy, 2nd ed., McGraw-Hill,1976

[7] S.L. Lehoczky, J Appl Phys 49 (1978) 5479.

[8] K.K. Shih and D.B. Dove, "Ti/Ti-N Hf/Hf-N and W/W-N multilayer films with high mechanical hardness" Appl. Phys. Lett. **61** (1992) 654-6

[9] X. Chu, M.S. Wang, W.D. Sproul, S.L. Rohde, S.A. Barnett, J Vac Sci Technol A 10(4) (1992) 1604.

[10] U. Helmersson, S. Todorova, S.A. Barnett, J.E. Sundgren, L.C. Markert and J.E. Greene, "Growth of single-crystal TiN/VN strained-layer superlattices with extremely high mechanical hardness", J. Appl. Phys. **62** (1987) 481-4.

[11] D.C. Cameron, R. Aimo, Z.H. Wang and K.A. Pischow, " Structural variations in CrN/NbN superlattices", Surf. Coat. Technol. **142-144** (2001) 567-72.

[12] J. Lin, J.J. Moore, B. Mishra, M. Pinkas, W.D. Sproul, "Nano-structured CrN/AlN multilayer coatings synthesized by pulsed closed field unbalanced magnetron sputtering", Surface & Coatings Technology 204 (2009) 936–940.

[13] J. Lin, J.J. Moore, B. Mishra, M. Pinkas, X.H. Zhang, W.D. Sproul, "CrN/AlN superlattice coatings synthesized by pulsed closed field unbalanced magnetron sputtering with different CrN layer thicknesses", Thin Solid Films 517 (2009) 5798–5804.

[14] M. Nordin, M. Larsson, S. Hogmark, "Mechanical and tribological properties of multilayered PVD TiN/CrN", Wear 232 (1999) 221-225.

[15] L.S. Palatnik, A.I. Il'inskii, and N.P. Sapelkin, Sov. Phys. Solid State 8, 2016 (1967)

[16] J.S. Koehler, Attempt to Design a Strong Solid, Phys. Rev. B, 2, 547-551 (1970).

[17] J. Lin, J.J. Moore, B. Mishra, M. Pinkas, W.D. Sproul, "Nano-structured CrN/AlN multilayer coatings synthesized by pulsed closed field unbalanced magnetron sputtering", Surf. Coat. Technol. 204 (2009) 936-940

[18] J. Lin, J.J. Moore, W.C. Moerbe, M. Pinkas, B. Mishra, G.L. Doll, W.D. Sproul, "Structure and properties of selected (Cr-Al-N, TiC-C, Cr-B-N) nanostructured tribological coatings", Special issue on 'Tribology of Hard Coatings' in International Journal of Refractory Metals and Hard Materials, 28(1) (2009) 2-14.

[19] J. Lin, J. J. Moore, M. Pinkas, D. Zhong and W. D. Sproul, "TiBCN:CNx multilayer coatings deposited by pulsed closed field unbalanced magnetron sputtering", Surf. Coat. Technol. 206 (2011) 617-622

[20] J. Lin, I-W. Park, B. Mishra, M. Pinkas, J. J. Moore, J.M. Anton, K-H Kim, A.A. Voevodin, A. Levashov, "Processing, Structure, and Properties of Nanostructured Multifunctional Tribological Coatings", J. Nanoscience and Nanotechnology, 9 (2009) 4073-4084

[21] J. Lin, S. Myers, B. Mishra, J.J. Moore, and P. Ried, "Optimization of a Graded, Multilayer Die Coating System for Use in Al Pressure Die Casting", 111th Metalcasting Congress, Huston, May, (2007).

[22] J. Lin, S. Myers, B. Mishra, J.J. Moore, and P. Ried, "An examination of Coating Architecture in the Development of an Optimized Die Coating System for Aluminum Pressure Die Casting", 112th Metalcasting Congress, Atlanta, May, (2008)

[23] V.A. Koptsik and I.S. Rez, Pierre Curie's works in the field of crystal physics, Sov. Phys. Usp. 24 (5), (1981)

[24] M. J. Schulz, A. D. Kelkar, and M. J. Sundaresan, Nanoengineering of Structural, unctional, and Smart Materials, CRC press, New York, (2006).

[25] K.C. Kao, Dielectric Phenomena in Solids, Academic Press, London (2004)

[26] Z. An, C. Men, Z. Xu, P. K. Chu and C. Lin, "Electrical properties of AlN thin films prepared by ion beam enhanced deposition", Surface & Coatings Technology, 196 (2005)

[27] J.G. Simmons, Conduction In Thin Dielectric Films, J. Phys. D: Appl. Phys., vol 4, (1971) 613.

[28] L. Goux, D.J. Wouters, "Imprint mechanism in integrated bi-rich SrBi2Ta2O9 capacitors: influence of the temperature-dependent polarization", J. Appl. Phys., vol 100, No.12, (2006) 124102.

[29] P. Muralt, "Ferroelectric thin films for micro-sensors and actuators: a review", J. Micromech. Microeng., vol 10, (2000) 136.

[30] A.J. Moulson, and J.M. Herbert, Electroceramics, Chapman and Hall, London, (1990).

[31] O.J. Gregory, A.B. Slot, P.S. Amons and E.E. Crisman, "High temperature strain gages based on reactively sputtered AlNx thin films", Surface and Coatings Technology, vol 88, (1996) 79

[32] A.Barker, S. Crowther, and D. Rees, "Room-temperature r.f. magnetron sputtered ZnO for electromechanical devices", Sensors and Actuators A, vol 58, (1997) 229.

[33] M. Tomar, V. Gupta, A. Mansingh and K. Sreenivas, "Temperature Stability of c-axis Oriented $LiNbO_3/SiO_2/Si$ Thin Film Layered Structures", J. Phys. D: Appl. Phys., vol 34, No. 15, (2001) 2267.

[34] X.H. Xu, , Xi'an, "Morphological properties of AlN piezoelectric thin films deposited by DC reactive magnetron sputtering", Thin Solid Films, Vol. 388 (2000).

[35] J. A. Ruffner, P. G. Clem, B. A. Tuttle, D. Dimos, and D. M. Gonzales, Thin Solid Films 354, (1999) 256

[36] H. Baránkova and L. Bardos, Surf. Coat. Technol. 120–121, (1999) 704.

[37] A. Matthews, Plasma-based PVD Surface Engineering Processes, J. Vac. Sci. Technol, A 21(5), (2003) S224.

[38] W. D. Sproul, P. J. Rudnik, M. E. Graham, and S. L. Rohde, "High-rate Reactive Sputtering in An Ppposed Cathode Closed-field Unbalanced Magnetron Sputtering System", Surf. Coat. Technol, 43, (1990) 270.

[39] S. L. Rohde, W. D. Sproul, and J. R. Rohde, "Correlations of Plasma and Magnetic Field Characteristics to TiN Film Properties Formed Using a Dual Unbalanced Magnetron System", J. Vac. Sci. Technol, A 9(3), (1991) 1178.

[40] K. Tominaga, "Preparation of AIN Films by Planar Magnetron Sputtering System with Facing Two Targets", Vacuum 41 (1990) 1154-1156.

[41] A.J. Perry, J.A. Sue, and P.J. Martin, Surf. Coat. Technol. 81, (1996) 17.

[42] I.C. Noyan, and J.B. Cohen, Residual Stress Measurement by Diffraction and Interpretation, Springer-Verlag, New York (1987).

[43] V. Srivastara, R. Joshi, R. Shivpuri, R. Bhattacharya, S. Dixit, Surf. Coat. Technol. 163, (2003) 631.

[44] I. Petrov, F. Adibi, J.E. Greene, L. Hultman, and J.-E. Sundgren, Appl. Phys. Lett. 63(1), (1993) 36.

[45] J. Lin, J.J. Moore, B. Mishra, W.D. Sproul, and J.A. Rees, Surf. Coat. Technol. 201, (2007) 4640.

[46] J. Lin, B. Mishra, J.J. Moore, W.D. Sproul, Surf. Coat. Technol. 201 (2006) 4329.

[47] J. Lin, Z.L. Wu, X.H. Zhang, B. Mishra, J.J. Moore, W.D. Sproul, Thin Solid Films, 517 (2009) 1887.

[48] X. Chu and S.A. Barnett, J Appl Phys 77(9) (1995) 4403.

[49] S.L. Lehoczky, J Appl Phys 49 (1978) 5479.

[50] W. Heinke, A. Leylan, A. Matthews, G. Berg, C. Friedrich, E. Broszeit, Thin Solid Films 270 (1995) 431.